Chapter 19
Cryogenic Detectors

Klaus Pretzl

19.1 Introduction

Most calorimeters used in high energy physics measure the energy loss of a particle in form of ionization (free charges) or scintillation light. However, a large fraction of the deposited energy in form of heat remains undetected. The energy resolution of these devices is therefore mainly driven by the statistical fluctuations of the number of charge carriers or photoelectrons involved in an event. In contrast, cryogenic calorimeters are able to measure the total deposited energy including the heat in form of phonons or quasi-particles in a superconductor. With the appropriate phonon or quasi-particle detection system much higher energy resolutions can be obtained due to the very large number of low energy quanta (meV) involved in the process. This feature makes cryogenic calorimeters very effective in the detection of very small energy deposits (eV) with resolutions more than an order of magnitude better than for example semiconductor devices.

During the last two decades cryogenic detectors have been developed to explore new frontiers in physics and astrophysics. Among these are the quest for the dark matter in the universe, the neutrinoless double beta decay and the mass of the neutrino. But other fields of research have also benefited from these developments, such as astrophysics, material and life sciences.

The calorimetric measurement of deposited energy in an absorber dates back to 1878, when the American astronomer S.P. Langley invented the bolometer [1]. With this device he was able to measure the energy flow of the sun in the far infrared region of the spectrum and to determine the solar constant. Since then the bolometer has played an important role to measure the energy of electromagnetic radiation

K. Pretzl (✉)
Laboratory for High Energy Physics - Albert Einstein Center for Fundamental Physics, University of Bern, Bern, Switzerland
e-mail: pretzl@lhep.unibe.ch

C. W. Fabjan, H. Schopper (eds.), *Particle Physics Reference Library*,
https://doi.org/10.1007/978-3-030-35318-6_19

of celestial objects. At the turn of the century radioactivity was discovered and P. Curie and A. Laborde made a first attempt in 1903 to measure the energy released in radioactive decays using a calorimetric device [2]. Thereafter micro-calorimeters were developed by C.D. Ellis and A. Wooster in 1927 [3] and independently by W. Orthmann and L. Meitner in 1930 [4] to determine the average energy of the electron in the beta-decay of ^{210}Bi. The differential micro-calorimeter developed by W. Orthmann allowed to measure heat transfers of the order of μW. Using this true calorimetric technique, he and L. Meitner were able to determine the average energy of the continuous beta spectrum in ^{210}Bi to 0.337 MeV with a 6% accuracy. These measurements contributed greatly to the notion of a continuous beta-spectrum leading to W. Pauli's neutrino hypothesis in 1930.

In 1935 F. Simon [5] suggested to measure the energy deposited in radioactive decays with low temperature calorimeters. He claimed that with a calorimeter of 1 cm^3 tungsten in a liquid helium bath at 1.3 K, one could measure a heat transfer of nW, which is about 1000 times more sensitive than the calorimeter of W. Orthmann. The argument is that at low temperatures the heat capacity C of a micro-calorimeter is low and a small energy loss E of a particle in the calorimeter can lead to an appreciable temperature increase $\Delta T = E/C$. Later in 1949, D.H. Andrews, R.D. Fowler and M.C. Williams [6] reported the detection of α-particles from a Po source with a bolometer made of a superconducting strip of NbN mounted on a copper base. The operating temperature was chosen 15.5 K, which corresponded to the center of the transition halfway between the superconducting and the normal state of NbN. However, at this stage of the experiment no energy information of the alpha particles could be extracted from the signals, since the signal to background ratio was not sufficient. Their bolometer was used only as a particle counter. In 1969, G.H. Wood and B.L. White [7] were able to measure the energy of the emitted alpha particles from a polonium source with a superconducting tunnel junction (STJ). The energy was derived from the tunneling current, which is proportional to the excitations of the quasi-particles induced by the energy loss of the α-particles in the junction.

H. Bernas et al. [8] introduced 1967 superheated superconducting granules (SSG) to measure beta radiation. Used as an energy threshold detector the energy loss of an electron in a granule could suffice to drive the granule from a super-conducting into a normal state. This phase transition would induce a signal in a pickup coil due to the Meissner effect, provided the granules are sitting in an external magnetic field. A. Drukier and C. Vallette [9] were able to detect charged particles with a SSG device. Later in 1984, A. Drukier and L. Stodolsky [10] suggested the use of SSG detectors for neutrino and astrophysics experiments.

In early 1970 a new type of bolometer, the so-called composite one, was developed by N. Coron, G. Dambier and J. Leblanc [11]. It consisted of an absorber and a thermally coupled thermometer in form of a semiconductor thermistor. Later in 1974, T. Niinikosky and F. Udo [12] proposed cryogenic calorimeters for the detection of neutrinos. E. Fiorini and T. Niinikoski [13] explored in 1984 the possibility of using low temperature bolometers to improve the limits on neutrinoless double beta decays. At this time D. McCammon, S.H. Moseley, J.C. Mather and R. Mushotzky [14] published first results with a cryogenic calorimeter

for X-ray spectroscopy. In 1985 N. Coron et al. [15] developed a cryogenic composite bolometer as a charged particle spectrometer.

Based on all these interesting ideas and developments, a first workshop on low temperature detectors (LTD1) was held in 1987 at Ringberg-Castle on Lake Tegernsee in southern Bavaria. Due to the success of this workshop and the growing interest in this field, further workshops have been organized in Europe, the USA and Japan. Much of the original work in this field can be found in the proceedings of these LTD workshops [16–31]. There exist also excellent review articles [32–37] as well as a textbook [38] on this subject.

19.2 General Features of Cryogenic Calorimeters

A typical cryogenic calorimeter is shown in Fig. 19.1. It consists of three basic elements: an absorber, which confines the interaction volume, a thermometer, which is thermally well coupled to the absorber and which measures the temperature increase due to the energy loss of a particle in the absorber, and a thermal bath, which has a weak thermal link to the absorber and restores the temperature in the absorber to a defined base value. Particles interacting in the absorber material lose their energy in producing atomic and solid state excitations. These excitations produce electrons, photons (photoelectrons) and phonons. Phonons are quantized lattice vibrations which behave like particles and propagate with the speed of sound. The energy of these particles will degrade in time via electron-phonon and phonon-

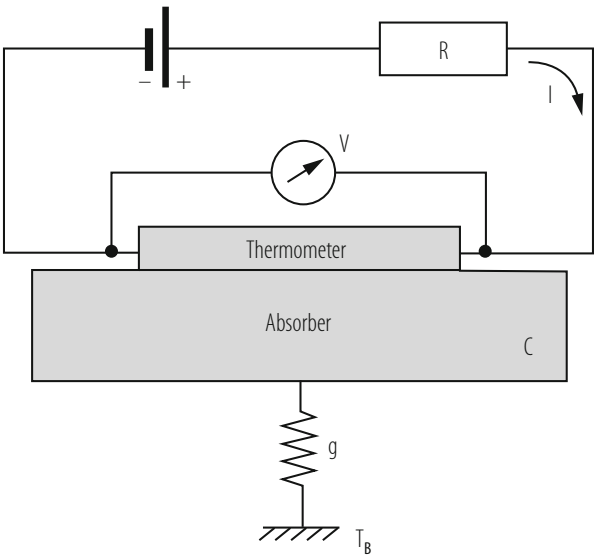

Fig. 19.1 The principle of a cryogenic calorimeter is shown

phonon interactions as well as via interactions with lattice irregularities until the system settles in thermal equilibrium. Calorimeters operating in the equilibrium mode (i.e. being sensitive to thermal phonons) offer in principle the best energy resolution, because the number of thermal phonons, with typical energies of meV, is large and the statistical fluctuations are small. For some applications thermal detectors can also be used in a non-equilibrium mode being sensitive to only high energy, so-called quasi-ballistic, phonons. These devices have the advantage of being intrinsically faster, but with energy resolutions inferior to equilibrium detectors. In calorimeters made from superconducting materials, such as superconducting tunnel junctions, the excitation energy is transformed into phonons as well as quasi-particles. These devices operate in the non-equilibrium mode, since the excitations (quasi-particles) are measured before they settle in thermal equilibrium. As described in more detail in the following paragraphs, most low temperature calorimeters differ in the way they are converting the excitation energy into a measurable signal.

Assuming that the deposited energy E of a particle in the absorber is fully thermalized the temperature rise ΔT is given by:

$$\Delta T = \frac{E}{C_{tot}}\,, \tag{19.1}$$

where $C_{tot} = cV$ is the heat capacity of an absorber with the volume V and the specific heat c. Cryogenic detectors operate at low temperatures because the heat capacity of many absorber materials becomes very small leading to an appreciable temperature rise. In addition the absorber volumes are kept as small as possible, in some cases of mm^3 or cm^3 size. Therefore they are also often called microcalorimeters. Applying the Debye model to calculate the internal energy of the lattice vibrations (phonons), the specific heat of a dielectric crystal absorber comes out to be:

$$c_{dielectric} = \beta(\frac{T}{\theta_D})^3\,, \tag{19.2}$$

with $\beta = 1944\ \mathrm{J\ mol^{-1}\ K^{-1}}$ and θ_D the Debye temperature of the crystal. The cubic dependence on temperature demonstrates a strong decrease of the phonon specific heat at low temperatures. In a metal absorber there are two components which determine the specific heat: lattice vibrations and thermally excited conduction electrons. The specific heat of a normal conducting material at low temperatures is given by:

$$c_{metal} = \beta(\frac{T}{\theta_D})^3 + \gamma T\,, \tag{19.3}$$

with γ being a material dependent constant (Sommerfeld constant). At temperatures below 1 K the electronic specific heat dominates. Therefore the total specific heat

decreases only linearly with temperature. Another frequently used absorber is a superconductor. In this case the specific heat consists of a term due to lattice vibrations and a second term which reflects the number of thermally excited electrons across the energy gap of a superconductor Δ. The latter diminishes exponentially with temperature due to the decrease of the quasi-particle density:

$$c_{supercond.} = \beta(\frac{T}{\theta_D})^3 + a \exp\left\{(-\frac{b\Delta}{k_B T})\right\}, \tag{19.4}$$

with a and b being material constants and k_B is the Boltzmann constant. Therefore at very low temperatures the specific heat of a superconductor is dominated by lattice vibrations.

The characteristics of an ideal cryogenic calorimeter can be described by the heat capacity C of the absorber and the thermal conductivity g of the link to the heat bath with the temperature T_B. In the event of a particle losing an energy E in the absorber the temperature in the absorber will according to Eq. (19.1) rise by ΔT and then decay back to its starting temperature, which corresponds to the bath temperature T_B. The time constant of this process is given by $\tau = C/g$. The temperature rise in the absorber will change the resistance of the thermometer, which is measured by recording a voltage drop across it when passing a current I through the thermometer (Fig. 19.1). The same device can also be used to measure a continuous power input P in form of electromagnetic radiation for example. In this case the temperature rise is given by $\Delta T = P/g$. Such a device is usually referred to as a bolometer. Bolometers have a long tradition in detecting infrared radiation from astrophysical objects. They have also been used in the measurements of the cosmic microwave background radiation.

Cryogenic calorimeters can be made from many different materials including superconductors, a feature which turns out to be very useful for many applications. They can be used as targets and detectors at the same time. Due to the very small energy quanta involved they reach much higher energy resolutions than conventional ionization or solid state devices. For example, it takes only of the order of 1 meV to break a Cooper pair in a superconductor whereas a few eV are needed to create an electron-hole pair in a solid-state device. Cryogenic calorimeters are able to detect very small energy transfers, which makes them sensitive also to non-ionizing events.

The intrinsic energy resolution of a cryogenic calorimeter is limited by the thermal energy fluctuations due to the phonon exchange between the absorber and the heat sink. The mean square energy fluctuation is given by Chui et al. [43]:

$$< \Delta E^2 >= k_B T^2 C\,. \tag{19.5}$$

It is independent of the absorbed energy E, the thermal conductivity g of the heat link and the time constant τ. The above equation can intuitively be understood when assuming that the effective number of phonon modes in the detector is $N = C/k_B$, the typical mean energy of one phonon is $k_B T$ and the rms fluctuation of one phonon is one. Then the mean square energy fluctuation is $N(k_B T)^2 = k_B T^2 C$.

For a practical cryogenic calorimeter the energy resolution is therefore given to first order by

$$\Delta E_{FWHM} = 2.35\xi\sqrt{k_B T^2 C}\,, \tag{19.6}$$

where ξ is a parameter which depends on the sensitivity and noise characteristics of the thermometer and can have values between 1.2 and 2.0. The best resolution obtained so far with cryogenic calorimeters is ∼2 eV at 6 keV.

The use of superconductors as cryogenic particle detectors was motivated by the small binding energy 2Δ (order of meV) of the Cooper pairs. The breaking of a Cooper pair results in the creation of two excited electronic states the so-called quasi-particles. A particle traversing a superconductor produces quasi-particles and phonons. As long as the energy of the quasi-particles and the phonons is higher than 2Δ, they break up more Cooper pairs and continue to produce quasi-particles until their energy falls below the threshold of 2Δ. Particles which lose the energy E in an absorber produce ideally $N = E/\Delta$ quasi-particles. Thus the intrinsic energy resolution of a superconducting cryogenic calorimeter with $\Delta \approx 1$ meV is given by

$$\Delta E_{FWHM} = 2.35\sqrt{\Delta F E} \sim 2.6\ \text{eV} \tag{19.7}$$

for a 6 keV X-ray assuming a Fano factor $F = 0.2$, which is representative for most superconductors and which takes the deviation from Poisson statistics in the generation of quasi-particles into account.

For comparison, the energy resolution of a semiconductor device is typically:

$$\Delta E_{FWHM} = 2.35\sqrt{w F E} \sim 110\ \text{eV} \tag{19.8}$$

for a 6 keV X-ray, where w is the average energy necessary to produce an electron hole pair. It has a typical value of $w \approx 3$ eV. The Fano factor is $F = 0.12$ for Silicon. Because of the larger number of free charges a super-conducting device has a much better energy resolution.

In Fig. 19.2 X-ray spectra obtained with a state of the art Si(Li) solid-state device (dashed line) and a cryogenic micro-calorimeter (solid line) using a Bi absorber and an Al-Ag bilayer superconducting transition edge thermometer are compared. The micro-calorimeter has been developed at the National Institute of Standards and Technology (NIST) in Boulder (USA) [42].

19.3 Phonon Sensors

Phonons produced by a particle interaction in an absorber are far from thermal equilibrium. They must decay to lower energy phonons and become thermalized before the temperature rise ΔT can be measured. The time required to thermalize

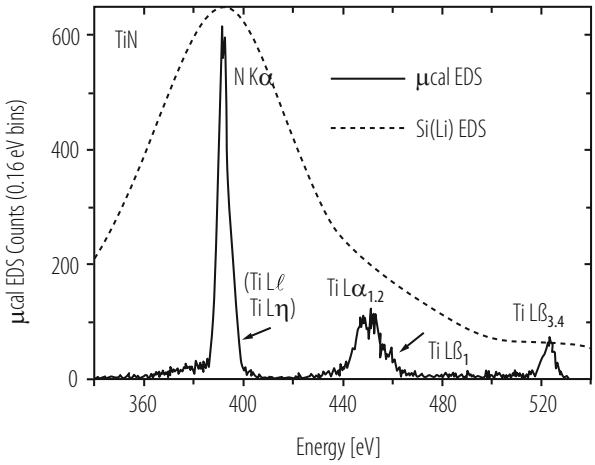

Fig. 19.2 TiN X-ray spectra obtained with a cryogenic micro-calorimeter (solid line) from the NIST group (see text) and with a state of the art Si(Li) solid-state device (dashed line) are compared. EDS stands for energy dispersive spectrometer. TiN is an interconnect and diffusion barrier material used in semiconductor industry

and the long pulse recovery time ($\tau = C/g$) limits the counting rate of thermal calorimeters to a few Hz. The most commonly used phonon sensors are resistive thermometers, like semiconducting thermistors and superconducting transition edge sensors (TES), where the resistance changes as a function of temperature. These thermometers have Johnson noise and they are dissipative, since the resistance requires power to be read out, which in turn heats the calorimeter (Joule heating). However, the very high sensitivities of these calorimeters can outweigh to a large extent these disadvantages. There are also magnetic thermometers under development, which do not have readout power dissipation.

19.3.1 Semiconducting Thermistors

A thermistor is a heavily doped semiconductor slightly below the metal insulator transition. Its conductivity at low temperatures can be described by a phonon assisted electron hopping mechanism between impurity sites. This process is also called "variable range hopping" (VRH) [44]. For temperatures between 10 mK and 4 K the resistance is expected to follow $R(T) = R_0 \exp\left\{(\frac{T_0}{T})^{\frac{1}{2}}\right\}$. This behavior is observed in doped Si and Ge thermistors. However, depending on the doping concentrations of the thermistor and the temperature range of its use, deviations from this behaviour have also been discovered. An important requirement for the fabrication of thermistors is to achieve a good doping homogeneity and reproducibility. Good uniformity of doping concentrations has been achieved either

with ion implantation or with neutron transmutation doping (NTD). In the latter case, thermal neutrons from a reactor are captured by nuclei which transform into isotopes. These can then be the donors or acceptors for the semiconductor. NTD Ge thermistors are frequently used because of their reproducibility and their uniformity in doping density. Furthermore they are easy to handle and commercially available.

It is convenient to define a dimensionless sensitivity of the thermometer:

$$\alpha \equiv \frac{d \log R}{d \log T} = \frac{T}{R} \frac{dR}{dT} . \tag{19.9}$$

The energy resolution of these devices is primarily driven by the heat capacity C of the absorber, the sensitivity of the thermometer α, the Joule heating, the Johnson noise of the load resistor and the amplifier noise. The bias current through the resistor can be optimized in such a way that it is kept high enough to provide a suitable voltage signal and low enough to minimize the Joule heating. If also the Johnson noise and the amplifier noise can be kept sufficiently low, the energy resolution of an ideal calorimeter can be described to first order by Eq. (19.6), where ξ is approximately $5(1/\alpha)^{1/2}$ [39]. For large values of α the energy resolution can be even much better than the magnitude of the thermodynamic fluctuations provided no power is dissipated by the temperature measurement of the sensor. Semiconducting thermistors have typically α values between 6 and 10, while superconducting transition edge sensors (TES) have values which are two orders of magnitude higher. A detailed description of the noise behavior and the energy resolution of cryogenic detectors can be found in [39–41].

19.3.2 Superconducting Transition Edge Sensors (TES)

A frequently used phonon sensor is the so-called transition edge sensor (TES). It consists of a very thin superconducting film or strip which is operated at a temperature in the narrow transition region between the superconducting and the normal phase, where its resistance changes between zero and its normal value R_N, as shown in Fig. 19.3a. TES sensors are usually attached to an absorber, but they can also be used as absorber and sensor at the same time. The very strong dependence of the resistance change on temperature, which can be expressed in the dimensionless parameter α of Eq. (19.9), makes the TES calorimeter sensitive to very small input energies. Superconducting strips with low T_c can have α values as high as 1000. This requires very high temperature stability. The Munich group has developed one of the first TES sensors, which was made from tungsten with a transition temperature of 15 mK [45].

The TES sensor can be operated in two different modes: the current and the voltage biased mode. In a current biased mode of operation a constant current is fed through the readout circuit as shown in Fig. 19.3b. A particle interaction in the absorber causes a temperature rise and a corresponding increase of the

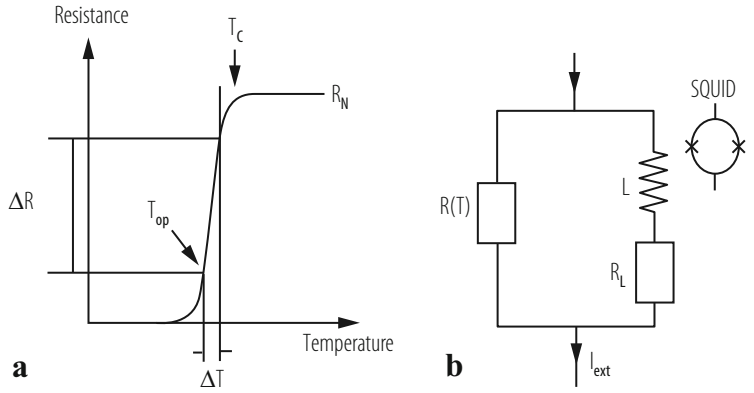

Fig. 19.3 (**a**) The temperature versus resistance diagram of a superconducting strip close to the transition temperature T_c is shown. (**b**) The dc-SQUID readout of a transition edge sensor is shown

resistance $R(T)$ of the attached TES sensor. The change of the resistance forces more current through the parallel branch of the circuit, inducing a magnetic flux change in L which is measured with high sensitivity by a superconducting quantum interference device (SQUID). However, in this mode Joule heating by the current through the sensor and small fluctuations in the bath temperature can prevent to achieve good detector performances. To solve this problem K.D. Irwin [46] has developed a so-called auto-biasing electro-thermal feedback system (ETF), which works like a thermal equivalent to an operation amplifier and keeps the temperature of the superconducting strip at a constant value within its transition region. When operating the transition edge sensor in a voltage biased mode (V_B), a temperature rise in the sensor causes an increase in its resistance and a corresponding decrease in the current through the sensor, which results in a decrease of the Joule heating ($V_B \cdot \Delta I$). The feedback uses the decrease of the Joule heating to bring the temperature of the strip back to the constant operating value. Thus the device is self-calibrating. The deposited energy in the absorber is given by $E = V_B \int \Delta I(t)dt$. It can directly be determined from the bias voltage and the integral of the current change. The use of SQUID current amplifiers allows for an easy impedance matching to the low resistance sensors and opens the possibility to multiplex the read out of large arrays of TES detectors. Another advantage of ETF is that in large pixel arrays the individual channels are self-calibrating and temperature regulated. Most important, ETF shortens the pulse duration time of TES by two orders of magnitude compared to thermistor devices allowing for higher count rates of the order of 500 Hz.

The intrinsic energy resolution for an ideal TES calorimeter is given by Eq. (19.6) with $\xi = 2(1/\alpha)^{1/2}(n/2)^{1/4}$, where n is a parameter which depends on the thermal impedance between the absorber (phonons) and the electrons in the superconducting film [46, 47]. For thin films and at low temperatures the electron-phonon decoupling dominates in the film and n is equal to 5. The best reported energy resolutions with TES devices so far are a little below 2 eV at 6 keV.

The observed transition width of TES ΔT in the presence of a typical bias current is of the order of a few mK. Large bias currents usually lead to transition broadenings due to Joule heating and self-induced magnetic fields. In order to achieve best performance of TES in terms of energy resolution or response time for certain applications, specific superconducting materials have to be selected. Both superconductors of type I and type II qualify in principle. However, the physics of the phase transition influences the noise behavior, the bias current capability and the sensitivity to magnetic field of the TES. Sensors made from high temperature superconductors have a much lower sensitivity than low temperature superconductors due to the larger gap energies Δ and heat capacities C. Thermal sensors made from strips of Al (with $T_c = 1.140$ K), Ti (0.39 K), Mo (0.92 K), W (0.012 K) and Ir (0.140 K) have been used. Ti and W sensors have been developed in early dark matter detectors [48–51]. But also other transition edge sensors, made from proximity bi-layers such as Al/Ag, Al/Cu, Ir/Au, Mo/Au, Mo/Cu, Ti/Au, or multi-layers such as Al/Ti/Au [56], have been developed to cover transition temperatures in the range between 15 and 150 mK. Although not all of these combinations are chemically stable, good detector performances have been obtained with Ir/Au bi-layers [52, 53] at transition temperatures near 30 mK. Methods to calculate bi-layer T_c can be found in [54, 55]. Another method to suppress the T_c of a superconducting film is to dope it with magnetic ions, like for example Fe ($<$100 ppm) [57]. However, there is a concern that the magnetic impurities may drastically increase the heat capacity of the film.

TES is also sensitive to non-thermal phonons with energies well above 2Δ. While losing energy these phonons produce quasi-particles before they thermalize. Since this process is very much faster than thermalization, signals of the order of µs can be achieved, enhancing considerably the counting rate capability of these devices as compared to thermal phonon sensors. Due to its high resolution and timing capabilities as well as versatile applications, TES sensors are currently among the most frequently used devices in calorimetric measurements. A detailed description of the performance of TES and ETF-TES can be found in [46, 47].

19.3.3 Magnetic Sensors

The magnetic properties of many materials are strongly dependent on temperature. This feature has been used to build very sensitive magnetic calorimeters applying thermal sensors made from thin paramagnetic strips, placed in a small magnetic field, which are in strong thermal contact with a suitable particle absorber. The energy deposited in the absorber leads to a temperature rise and a corresponding decrease in magnetization of the sensor. The change of magnetization is given by

$$\Delta M = \frac{dM}{dT}\frac{\Delta E}{C_{tot}} \tag{19.10}$$

with C_{tot} the total heat capacity of the thermometer and the absorber. It can be very accurately measured with a high bandwidth dc-SQUID magnetometer. The use of magnetism as thermal sensor was first developed by Buehler and Umlauf [58] and Umlauf and Buehler [59]. In these first attempts magnetic calorimeters were using the magnetization of 4f ions in dielectric host materials to measure temperature changes. Due to the weak coupling of the magnetic moments to the phonons at low temperatures these devices exhibited a too slow response time (order of seconds) for many applications. This problem was overcome by introducing sensors which use magnetic ions in metallic base material [60]. This type of device is called metallic magnetic calorimeter (MMC). In metals the relaxation times due to interactions between conduction electrons and magnetic moments are orders of magnitude faster than in dielectrics. However, the presence of conduction electrons increases the heat capacity of the sensor and leads to an enhanced interaction amongst magnetic moments. Nevertheless, very promising results were obtained with a metallic magnetic calorimeter [61]. It consisted of two thin Au disc sensors (50 µm in diameter and 25 µm thick) containing 300 ppm enriched ^{166}Er and a gold foil ($150 \times 150 \times 5\,\mu m^3$) as an X-ray absorber. The calorimeter reached an energy resolution of 3.4 eV at 6 keV, which is quite comparable to TES and thermistor calorimeters. An important property of MMC is that its inductive read out, which consists of a primary detector SQUID and a secondary SQUID amplifier, does not dissipate power into the system [61]. This feature makes MMC very attractive for many applications, in particular where large pixel arrays are of interest. The energy resolution of MMC is primarily driven by the thermal conductance between the absorber and the temperature bath and between the absorber and the sensor. For an ideal MMC the energy resolution is then given by Eq. (19.6), where ξ is approximately $\xi = 2\sqrt{2}(\tau_0/\tau)^{1/4}$ with τ_0 (typically order of µs) the relaxation time between the absorber and the sensor and τ (typically order of ms) the relaxation time between the absorber and the bath temperature [62]. It is further assumed that the heat capacities of the absorber and the sensor are approximately equal. In this case the heat capacity C in Eq. (19.6) represents the heat capacity of the absorber. MMC devices have potential applications in X-ray spectroscopy and are under further development for large pixel array cameras.

19.4 Quasiparticle Detection

The physics of superconducting detectors are based on Cooper pair breaking and quasi-particle production. Quasi-particles created by the absorption of X-rays or by the energy loss of a transient particle in a superconducting absorber can be measured with a Superconducting Tunnel Junction (STJ). The STJ device is in principle the same as the more widely known Josephson junction [63]. When biasing the STJ at a suitable voltage the tunneling current through the junction is proportional to the excess number of quasi-particles produced. To be able to measure these excess quasi-particles above the thermal background one has

to go to very low temperatures $T < 0.1\,T_c$. Arrays of STJs are also used to measure high energy, non-thermal (ballistic) phonons produced in either a dielectric or superconducting absorber. A new detector concept, called microwave kinetic inductance detector (MKID), has been developed which allows a frequency-domain approach to multiplexing and results in a dramatic simplification of the array and its associated readout electronics. Another detection scheme is based on small superheated superconducting granules (SSG) embedded in an external magnetic field. They are kept just below the phase-transition border and will change from the superconducting to the normal-conducting phase upon thermal excitation, which leads to the breaking of Cooper pairs and the penetration of the external magnetic field into the granule, causing a magnetic flux change (Ochsenfeld-Meissner effect). The flux change can be measured with an appropriate pickup coil. All these detectors are non-equilibrium devices.

19.4.1 Superconducting Tunnel Junctions (STJ)

The pioneering work of the groups of the Paul Scherrer Institute (at Villigen, Switzerland) [64] and of the Technical University Munich (Germany) [65] and their promising first results have stimulated other institutes to further develop STJs for high resolution X-ray detection. A typical STJ consists of two superconducting films S1 and S2 with a thickness of a few nm separated by a thin, 1–2 nm thick, tunnel barrier, which is usually the oxide of one of the superconductors. Because of its structure the device is frequently referred to as SIS (superconductor/insolator/superconductor) junction, also sometimes called Giaever junction. Typical junction areas are of the order of $100 \times 100\,\mu\text{m}^2$. As a quasi-particle detector, the STJ is operated with a bias voltage which is usually set to be less than Δ/e, where e is the charge of an electron. The principle processes taking place in a STJ are illustrated in Fig. 19.4, which is taken from [67]. In the event of an incident particle

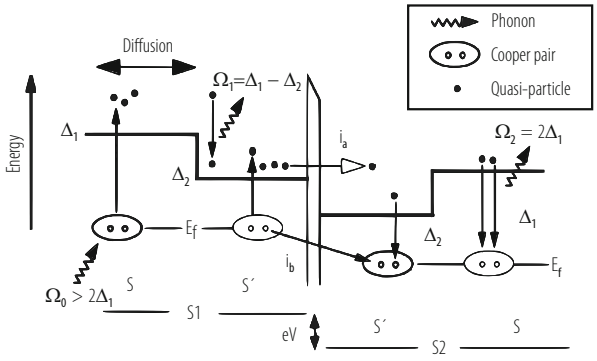

Fig. 19.4 The processes in a superconducting tunnel junction (ST) are illustrated

or X-ray interaction in film S1 the quasi-particle density is increased. This will lead to an increase of a net quasi-particle transfer from S1 to S2 and consequently to an increase of the tunneling current. However, not all quasi-particles will reach and pass through the junction barrier. Depending on the geometry and structure of the junction there will be losses. Quasi-particles can recombine to Cooper pairs radiating phonons as consequence of the relaxation process. If the phonon energy is high enough $\Omega_0 > 2\Delta_1$ to break new Cooper pairs, this process can lead to quasi-particle multiplication enhancing the signal output of the STJ. If, however, the phonon energy is below the energy threshold for breaking a Cooper pair $\Omega_0 < 2\Delta_1$ the quasi-particle will be lost and will not contribute to the signal. Quasi-particles will also be lost when they diffuse out of the overlap region of the junction films into the current leads instead of crossing the junction barrier. N. Booth [68] proposed a scheme which allows to recover some of these losses by quasi-particle trapping and in some cases quasi-particle multiplication. Quasi-particle trapping can be achieved by introducing bi-layers of superconducting materials (S(Δ_1) and S'(Δ_2)) with different gap energies $\Delta_2 < \Delta_1$ [68]. For example, an X-ray absorbed in the superconductor S produces phonons of energy $\Omega_0 > 2\Delta_1$ breaking a number of Cooper pairs. Some of the produced quasi-particles diffuse to the superconducting film S' of the STJ with a smaller gap energy Δ_2. By falling in that trap they relax to lower energies by emitting phonons, which could generate additional quasi-particles in the film S' (quasi-particle multiplication) if their energy is larger than $2\Delta_2$. However, the relaxed quasi-particles cannot diffuse back into the superconductor S because of their lower energy. They are trapped in S' and will eventually tunnel through the STJ, contributing to the signal with the tunneling current i_a. In order for quasi-particle trapping to be effective superconducting absorber materials with long quasi-particle lifetimes have to be selected (for example Al). Back tunneling, the so-called Gray effect, is also enhancing the signal [69]. In this Cooper pair mediated process a quasi-particle in film S2 recombines to form a Cooper pair at the expense of a Cooper pair in film S1. In this case the quasi-particle current i_b is also running in the direction of decreasing potential. Thus both excess quasi-particle currents i_a and i_b have the same sign. This feature allows to record signals from X-rays absorbed in either superconducting films S1 or S2 with the same sign. However, their signal shapes may not necessarily be the same due to different quasi-particle and tunneling losses in the two films. There are two other ways of electrical transport through the tunnel barrier which need to be suppressed when the STJ is used as a particle detector. One is the so-called dc Josephson current of Cooper pairs through the tunnel barrier. This current can be suppressed by applying a magnetic field of the order of a few Gauss parallel to the insulating barrier. The second is the tunnel current generated by thermally excited excess quasi-particles. The number density of these quasi-particles is decreasing with decreasing temperature according to $N_{th} \sim T^{1/2} \exp(-\Delta / k_B T)$. In order to obtain a significant signal to background ratio the operating temperature of a STJ detector should be typically lower than $0.1\ T_c$. The intrinsic energy resolution of the excess quasi-particles in a STJ device is given by Eq. (19.7), where Δ has to be replaced by ϵ, the effective energy needed to create one excited state. It turns out that $\epsilon \sim 1.7\ \Delta$ for Sn and Nb superconductors,

reflecting the fact that only a fraction of the absorbed energy is transfered into quasi-particles [70]. The number of quasi-particles generated in the STJ by an energy loss E of a particle in the superconductor is thus $N = E/\epsilon$. For a Nb superconductor with a Fano factor $F = 0.2$ and $\epsilon = 2.5\,\text{meV}$ one would expect from Eq. (19.7) an energy resolution of 4 eV at 6 keV. However, the best resolution observed so far is 12 eV at 6 keV. In order to estimate a more realistic energy resolution, quasi-particle loss and gain processes have to be taken into account. The two most important parameters driving the energy resolution of the STJ are the tunneling rate $\Gamma_t \equiv \tau_t^{-1}$ and the thermal recombination rate $\Gamma_r \equiv \tau_r^{-1}$. The temperature dependence of the thermal recombination rate is given by

$$\tau_r^{-1}(T) = \tau_0^{-1}\sqrt{\pi}\left(\frac{2\Delta}{k_B T_c}\right)^{5/2}\sqrt{\frac{T}{T_c}}\exp\left\{(-\frac{\Delta}{k_B T})\right\} \tag{19.11}$$

where τ_0 is the characteristic time of a superconductor. It has the values $\tau_0 = 2.3\,\text{ns}$ for Sn, $\tau_0 = 438\,\text{ns}$ for Al and $\tau_0 = 0.15\,\text{ns}$ for Nb [71].

The recombination rate $\Gamma_r \equiv \tau_r^{-1}$ can be minimized when operating the detector at sufficiently low temperatures, typically at $0.1\,T_c$, where the number of thermally excited quasi-particles is very small. The tunneling rate of a symmetric STJ is given by de Korte et al. [72]

$$\tau_t^{-1} = (4\,R_{norm}\cdot e^2\cdot N_0\cdot A\cdot d)^{-1}\frac{\Delta + eV_b}{\sqrt{(\Delta + eV_b)^2 - \Delta^2}} \tag{19.12}$$

where R_{norm} is the normal-conducting resistance of the junction, N_0 is the density of states of one spin at the Fermi energy, A is the junction overlap area, d the thickness of the corresponding film and V_b the bias voltage of the STJ. In practice, the tunneling time has to be shorter than the quasi-particle lifetime. For a $100\times100\,\mu\text{m}^2$ Nb-Al tunnel junctions with $R_{norm} = 15\,\text{m}\Omega$ a tunneling time of $\tau_t = 220\,\text{ns}$ and a recombination time of $\tau_r = 4.2\,\mu\text{s}$ has been measured [66]. The recombination time was determined from the decay time of the current pulse. Thus quasi-particles tunneled on average 19 times. In order to achieve even shorter tunneling times, one would have to try to further reduce R_{norm}. However, there is a fabricational limit avoiding micro-shorts in the insulator between the superconducting films. The STJ counting rate capability is determined by the pulse recovery time, which depends on the quasi-particle recombination time and can have values between several µs and up to ~50 µs. Typical count rates of STJs are 10^4 Hz. An order of magnitude higher count rates can still be achieved, but not without losses in energy resolution. The total quasi-particle charge collected in the STJ is to first order given by

$$Q = Q_0\frac{\Gamma_t}{\Gamma_d} \tag{19.13}$$

with $Q_0 = Ne$ and $\Gamma_d = 2\Gamma_r + \Gamma_{loss}$ the total quasi-particle loss rate. The factor 2 in the recombination rate takes into account the loss of two excited electronic states and Γ_{loss} stands for all the other quasi-particle losses, mainly due to diffusion. These effects can be parametrized into an effective Fano factor which is added into the equation for the energy resolution

$$\Delta E_{FWHM} = 2.35\sqrt{\epsilon(F+G)E}\,. \tag{19.14}$$

For a symmetric tunnel junction with equal tunneling probabilities on both sides the G factor is given by $G = (1 + 1/\bar{n})$ with $\bar{n} = Q/Q_0 = \Gamma_t/\Gamma_d$ [66, 67]. It emphasizes the importance of a large tunneling rate. Still the energy resolution in Eq. (19.14) is only approximative since it neglects gain factors like quasi-particle multiplication due to relaxation phonons and loss factors due to cancellation currents, which becomes important at low bias voltage.

From Eq. (19.12) it is clear that in order to achieve a high tunnel rate the STJ detector has to be made from very thin films with a small area A. These dimensions also determine the capacitance which should be kept as small as possible in order not to degrade the detector rise time and the signal to noise ratio. For the very thin films the quantum efficiencies at X-ray energies are very low. This can be changed by separating the absorber and detector functions in fabricating devices with a larger size superconducting absorber as substrate to a STJ. Quasi-particle trapping will be achieved when choosing substrate materials with a higher energy gap with respect to the junction.

Quasi-particle trapping was first demonstrated using a Sn absorber ($975 \times 150 \times 0.25\,\mu m^3$) with an energy gap of $\Delta_{Sn} = 0.58\,meV$ and with an Al-Al_2O_3-Al STJ at each end of the absorber [65]. Quasi-particles generated by an event in the Sn absorber diffuse into the aluminum junctions, where they stay trapped because of the smaller energy gap $\Delta_{Al} = 0.18\,meV$ of Al with respect to Sn. The excess quasi-particle tunnel current was then measured with the two Al STJs. In order to prevent diffusion losses out of the Sn absorber the common contact leads to the STJs and to the Sn absorber where made from Pb, which has an even higher energy gap of $\Delta_{Pb} = 1.34\,meV$. It turned out that more than 99.6% of the quasi-particles which tried to diffuse out of the absorber where rejected at the Pb barrier and hence confined to the absorber. Currently the best energy resolution of 12 eV at 6 keV has been achieved with a single Al-Al_2O_3-Al STJ using a superconducting Pb absorber ($90 \times 90 \times 1.3\,\mu m^3$) with an absorption efficiency of ≈50% [73]. It turns out that Al is an ideal material for STJ because it allows to fabricate a very uniform layer of the tunnel barrier and has a very long quasi-particle lifetime. These are features which are essential for a high performance STJ. A very good description of the physics and applications of STJ detectors can be found in [67].

Arrays of STJs have been developed for astronomical observations and other practical applications as discussed in the chapters below. The Naples collaboration [76] produced an array of circular shaped STJs [76, 77]. This device allows the operation of STJs without external magnetic field. Position sensitive devices have been developed for reading out large pixel devices [65, 74, 78].

19.4.2 Microwave Kinetic Inductance Detector

A new detector concept, called microwave kinetic inductance detector (MKID) has been introduced with the aim to develop multi-pixel array cameras for X-ray and single photon detection [79, 80]. MKID is, like STJ and SSG, a non-equilibrium detector which is based on Cooper pair breaking and the production of quasi-particles. The basic element of the device consists of a thin superconducting film, which is part of a transmission line resonator.

The principle of detection is shown in Fig. 19.5, taken from [79]: A photon absorbed in a superconducting film will break up Cooper pairs and produce quasi-particles (a). The increase of quasiparticle density will affect the electrical conductivity and thus change the inductive surface impedance of the superconducting film, which is used as part of a transmission line resonator (b). At resonance, this will change the amplitude (c) and the transmission phase of the resonator (d).

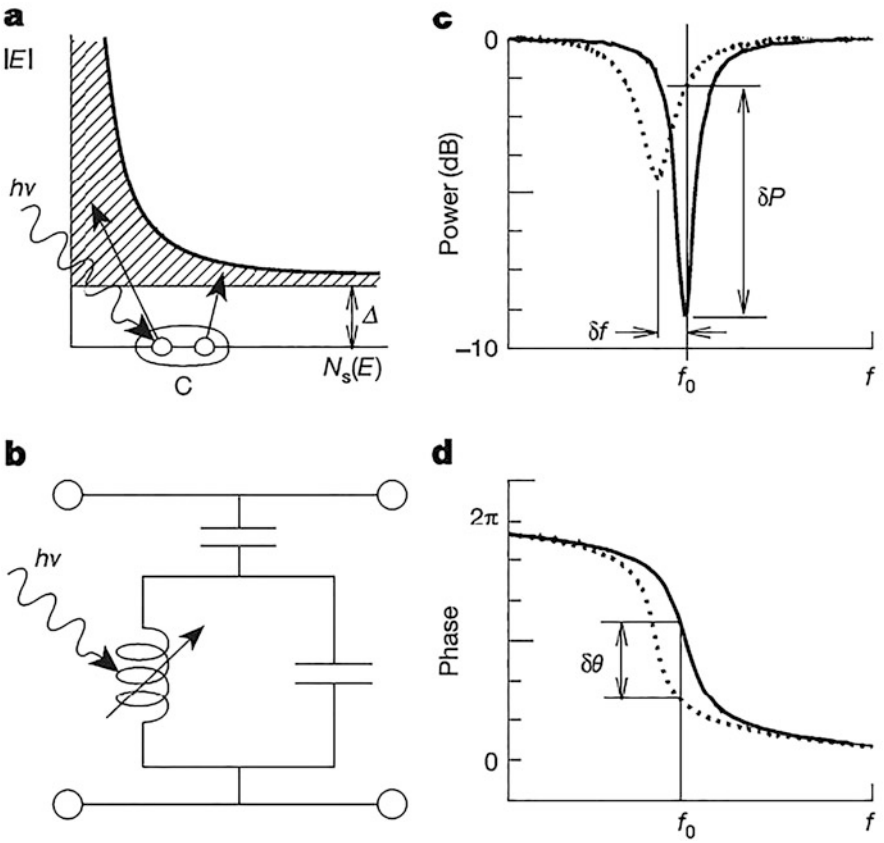

Fig. 19.5 The basic operation of a MKID (Microwave Kinetic Inductance Detector) is shown

The change in the transmission phase is proportional to the produced number of quasi-particles and thus to the photon energy. First measurements with an X-ray source yielded an energy resolution of 11 eV at 6 keV. MKID detectors find many applications where a large number of pixels are demanded. As compared to other devices multiplexing can be realized rather easy by coupling an array of many resonators with slightly different resonance frequencies to a common transmission line. A single amplifier is needed to amplify the signals from a large number of detectors. Due to its interesting features MKID is under development for many applications in ultraviolet, optical and infrared imaging [80].

19.4.3 Superheated Superconducting Granules (SSG)

Superheated superconducting granules (SSG) have been developed for X-ray imaging, transition radiation, dark matter as well as solar and reactor neutrino detection [10, 94]. A SSG detector consists of billions of small grains (typically 30 µm in diameter), diluted in a dielectric material (e.g. Teflon) with a volume filling factor of typically 10%. The detector is operated in an external magnetic field. Metastable type-1 superconductors (e.g. Sn, Zn, Al, Ta) are used, since their phase transitions from the metastable superconducting state to the normal-conducting state are sudden (in the order of 100 ns) allowing for a fast time correlation between SSG signals and those of other detectors. Its energy threshold is adjustable by setting the external magnetic field at a certain value ΔH just below the phase transition border. The phase diagram of a type-1 superconductor is schematically shown in Fig. 19.6, where H_{sh} is the superheating field, H_{sc} is the supercooling field and H_c is the critical thermodynamic field which is approximately given by $H_c(T) = H_c(0)(1 - (\frac{T}{T_c})^2)$. The region below H_{sc} is the superconducting and above H_{sh} the normal-conducting phase, while the region between the two is the so-called meta-stable phase, which is characteristic for superconductors of type-1. In order to keep the heat capacity as low as possible the SSG detector is operated at a temperature much below the critical temperature T_c at typically $T_0 \approx 100$ mK. Particles interacting in a granule produce quasi-particles. While spreading over the volume of the granule the quasi-particles are losing energy via electron-phonon interactions, thereby globally heating the granule up to a point where it may undergo a sudden phase transition (granule flip). The temperature change experienced by the granule is $\Delta T = \frac{3\Delta E}{4\pi c r^3}$, with ΔE the energy loss of the particle in the grain, c the specific heat and r the radius of the grain. The phase transition of a single grain can be detected by a pickup coil which measures the magnetic flux change $\Delta\Phi$ due to the disappearance of the Ochsenfeld-Meissner effect. In case of a single grain located in the center of the pickup coil the flux change is given by

$$\Delta\Phi = 2\pi B n \frac{r^3}{\sqrt{4R^2 + l^2}} \tag{19.15}$$

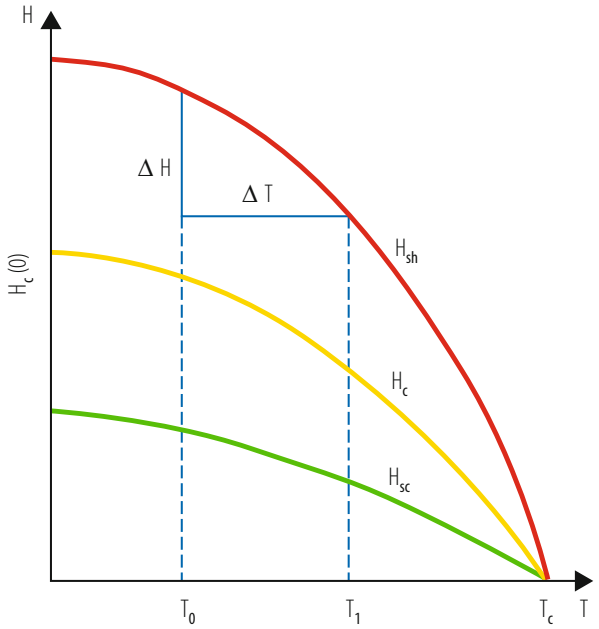

Fig. 19.6 The phase-diagram of a superconductor type1 is shown. H_{sh} is the superheating field, H_{sc} is the supercooling field and H_c is the critical thermodynamic field

with B the applied magnetic field, n the number of windings, R the radius and l the length of the pickup coil. It should be noted that one coil may contain a very large number of grains. If the flipping time τ is small compared to the characteristic time of the readout circuit ($\tau \ll 2\pi\sqrt{LC}$) the flux change induces a voltage pulse in the pick-up coil

$$V(t) = \frac{\Delta\Phi}{\omega LC} e^{-t/2RC} \sin(\omega t)\,, \quad \omega^2 = \frac{1}{LC} - \frac{1}{(2RC)^2} \tag{19.16}$$

with ω, L, R and C being parameters of the pick-up circuit. A detailed description of a readout concept using conventional pick-up coils and electronics including noise estimation is given in [81, 82]. Besides conventional readout coils more sensitive Superconducting Quantum Interference Devices (SQUID) were introduced [83–85]. The SQUID readout allows the detection of single flip signals from smaller size granules and/or the usage of larger size pickup coils. Granules of 20 µm diameter were measured in a large size prototype [85].

Small spherical grains can be produced at low cost by industry using a fine powder gas atomization technique. Since after fabrication the grains are not of a uniform diameter, they have to be sieved to select the desired size. A grain size selection within ±2 µm was achieved.

The Bern Collaboration has built and operated a dark matter SSG detector, named ORPHEUS, which consisted of 0.45 kg of spherical Sn granules with a diameter of ≈30 µm [81]. The detector was read out by 56 conventional pick-up coils, each 6.8 cm long and 1.8 cm in diameter. Each pick-up coil contained ≈80 million granules. The phase transition of each individual grain could be detected with a typical signal to noise ratio of better than 10. The principle to detect small nuclear recoil energies with SSG was successfully tested prior to the construction of the ORPHEUS detector in a neutron beam of the Paul Scherrer Institute (Villigen, Switzerland) [86]. The special cryogenics required for the ORPHEUS detector is described in [87]. The detector is located in the underground facility of the University Bern with an overburden of 70 meter water equivalent (m.w.e.). In its first phase the ORPHEUS dark matter experiment did not reach the sensitivity of other experiments employing cryogenic detectors, as described below. Further improvements on the superconducting behavior of the granules and on the local shielding are necessary.

SSG is a threshold detector. Its resolution depends on the sharpness $\delta H/H$, respectively $\delta T/T$, of the phase transition. It was found that the phase transition smearing depends on the production process of the grains. Industrially produced grains using the atomization technique exhibited a smearing of $\delta H/H \sim 20\%$. By using planar arrays of regularly spaced superheated superconducting microstructures which were produced by various sputtering and evaporation techniques the transition smearing could be reduced to about 2% [88–92]. The improvement of the phase transition smearing is one of the most important developments for future applications of SSG detectors. It looks promising that large quantities of planar arrays can be produced industrially [92].

There is a mechanism by which the energy transfered to a grain can be measured directly. If the grain is held in a temperature bath just below the H_{sc} boundary and the energy (heat) transfer to the grain is large enough to cross the meta-stable region to become normal-conducting, it will after some time cool down again to the bath temperature and become superconducting again. During this process the granule will provide a "flip" signal when crossing the H_{sh} border, and an opposite polarity "flop" signal when crossing the H_{sc} border. The elapsed time between the flip and the flop signal is a measure of the deposited energy in the grain. This effect has been demonstrated with a 11 µm Sn grain bombarded with α particles [93]. It offers the possibility to build an energy resolving and self-recovering SSG detector.

The practical realization of a large SSG detector is still very challenging. Nevertheless, the detector principle offers several unique features:

(a) The large list of suitable type-1 superconductor materials allows to optimize SSG for specific applications.
(b) Very low energy thresholds (eV) can be achieved.
(c) The inductive readout does not dissipate any power into the grains. Therefore the sensitivity of SSG is essentially determined by the grain size and the specific heat of the grain material.

(d) The sudden phase transitions are beneficial for coincident timing with other signals. Generally speaking, SSG detectors are among the most sensitive devices to detect very low energy transfers, i.e. nuclear recoils. A detailed description of SSG can be found in [10, 94, 95].

19.5 Physics with Cryogenic Detectors

19.5.1 Direct Dark Matter Detection

Among the most challenging puzzles in physics and cosmology is the existence of dark matter and dark energy. Dark matter, which was first inferred by Fritz Zwicky in 1933 [96], shows its presence by gravitational interaction with ordinary matter. It holds numerous galaxies together in large clusters and it keeps stars rotating with practically constant velocities around the centers of spiral galaxies. Dark energy, which was discovered by the Supernovae type 1a surveys in 1998 [97, 98], is driven by a repulsive force quite in contrast to the attractive gravitational force and causes the universe to expand with acceleration. The most recent information about the matter/energy content of the universe was gained from the Cosmic Microwave Background radiation (CMB) measurements by the Planck satellite [99]. According to these observations the universe contains 69.4% dark energy, 30.6% matter (including baryonic and dark matter) and 4.8% baryonic matter in form of atoms. The true nature of the dark energy and the dark matter, which fills about 95% of the universe, is still unknown. The direct detection of the dark energy, which is related to Einstein's cosmological constant, seems not to be in reach with present technologies. However, the direct detection of dark matter, if it exists in form of particles, is encouraged by the large expected particle flux which can be deduced under the following assumptions. In an isothermal dark matter halo model the velocity of particles in our galaxy is given by a Maxwell Boltzmann distribution with an average value of $< v >= 230\,\mathrm{km\,s^{-1}}$ and an upper cutoff value of $575\,\mathrm{km\,s^{-1}}$ corresponding to the escape velocity. The dark matter halo density in our solar neighborhood is estimated to be $\rho = 0.3\,\mathrm{GeV\ c^{-2}\,cm^{-3}}$. From that one expects a flux of $\Phi = \rho < v > /m_\chi \sim 7 \cdot 10^6/\mathrm{m}_\chi\,\mathrm{cm^{-2}\,s^{-1}}$ with m_χ the mass of the dark matter particle in $\mathrm{GeV\ c^{-2}}$. However, since neither the mass nor the interaction cross section of these particles are known one is forced to explore a very large parameter space, which requires very sensitive and efficient detection systems. The most prominent candidates for the dark matter are: massive neutrinos, WIMPs (weakly interacting massive particles) and axions. Neutrinos are among the most abundant particles in the universe, but their masses seem to be too small to contribute significantly to the missing mass. Neutrinos being relativistic at freeze out are free streaming particles, which cluster preferentially at very large scales. Therefore massive neutrinos would enhance large-scale and suppress small-scale structure formations. From hot dark matter and cold dark matter model calculations

fitting the power spectrum obtained from Large Scale Structure (LSS) surveys one obtains a value for the ratio neutrino density to matter density Ω_ν / Ω_m. From this value and Ω_m obtained from CMB an upper limit for the sum of the neutrino masses $\sum m_\nu \leq 0.234\,\mathrm{eV\ c^{-2}}$ can be derived. However, this and the results from direct neutrino mass experiments, as described below, indicate, that neutrinos have a mass to low to qualify for the dark matter. The introduction of axions was not motivated by cosmological considerations, but rather to solve the charge conjugation and Parity violation (CP) problem in Quantum Chromo-Dynamics (QCD) [100]. Nevertheless axions would be produced abundantly during the QCD phase transition in the early universe when hadrons were formed from quarks and gluons. A recent review of axion searches can be found in [101]. The most favored candidate for a WIMP is the neutralino, which is predicted by some Super Symmetric Theories (SUSY) to be the lightest stable SUSY particle. If the neutralino were to be discovered by the Large Hadron Collider (LHC) at CERN, it still would need to be confirmed as a dark matter candidate by direct detection experiments. However, up to now no sign of SUSY-particles has been observed at the LHC [102]. In the following the WIMP searches with some of the most advanced cryogenic detectors are described.

The direct detection of WIMPs is based on the measurement of nuclear recoils in elastic WIMP scattering processes. In the case of neutralinos, spin-independent coherent scatterings as well as spin-dependent scatterings are possible. The expressions for the corresponding cross sections can be found in [103, 104]. In order to obtain good detection efficiencies, devices with high sensitivity to low nuclear recoil energies (eV) are needed. WIMP detectors can be categorized in conventional and cryogenic devices. Most of the conventional WIMP detectors use NaI, Ge crystals, liquid Xenon (LXe) or liquid Argon (LAr). These devices have the advantage that large detector masses ($\sim$ton) can be employed, which makes them sensitive to annual modulations of the WIMP signal owing to the movement of the earth with respect to the dark halo rest frame. Annual modulation, if observed, would provide strong evidence for a WIMP signal, assuming it is not faked by spurious modulated background signals. However, due to quenching of the ionization signals, conventional detectors have lower nuclear recoil detection efficiencies than cryogenic devices.

Cryogenic detectors are able to measure small recoil energies with high efficiency because they measure the total deposited energy in form of ionization and heat. They can be made of many different materials, like Ge, Si, TeO_2, sapphire (Al_2O_3), LiF, $CaWO_4$ and BGO, including superconductors like Sn, Zn, Al, etc. This turns out to be an advantage for the WIMP search, since for a given WIMP mass the resulting recoil spectra are characteristically different for detectors with different materials, a feature which helps to effectively discriminate a WIMP signal against background. If the atomic mass of the detector is matched to the WIMP mass better sensitivity can be obtained due to the larger recoil energies. In comparison to conventional detectors, however, cryogenic detectors are so far rather limited in target mass ($\sim$kg).

Dark matter detectors have to be operated in deep underground laboratories in order to be screened from cosmic-ray background. In addition they need to be shielded locally against radioactivity from surrounding rocks and materials. The shielding as well as the detector itself has to be fabricated from radio-poor materials, which turns out to be rather expensive and limited in its effectiveness. Nevertheless, cryogenic detectors are capable of active background recognition, which allows to discriminate between signals from background minimum ionizing particles, i.e. Compton electrons, and signals from genuine nuclear recoils by a simultaneous but separate measurement of phonons and ionization (or photons) in each event. For the same deposited energy the ionization (or photon) signal from nuclear recoils is highly quenched compared to signals from electrons. The dual phonon-ionization detection method, which was first sugested by Sadoulet [105] and further developed by the CDMS and EDELWEISS collaborations, increases the sensitivity for WIMP detection considerably. A similar idea using scintillating crystals as absorbers and simultaneous phonon-photon detection was introduced by Gonzales-Mestres and Perret-Galix [106] and further developed by the ROSEBUD [107] and CRESST II [108] collaborations. The principle of the method is demonstrated in the scatterplot of Fig. 19.7, taken from [108]. It shows the energy equivalent of the pulse heights measured in the light detector versus those measured in the phonon detector. The scintillating $CaWO_4$ crystal absorber was irradiated with photons and electrons (using Cobalt and Strontium sources respectively) as well as with neutrons (using an Americium-Beryllium source). The photon lines visible in Fig. 19.7 were used

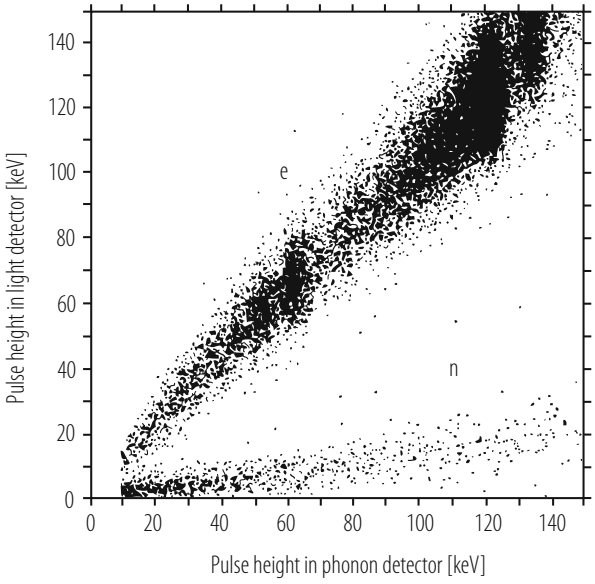

Fig. 19.7 The energy equivalent of the pulse heights measured with the light detector versus those in the phonon detector under electron, photon (e) and neutron (n) irradiation are shown

for the energy calibration in both the light and the phonon detector. The upper band in Fig. 19.7 shows electron recoils (e) and the lower band the nuclear recoils (n). Above an energy of 15 keV 99.7% of the electron recoils can be recognized and clearly distinguished from the nuclear recoils. Active background rejection was also practiced with the ORPHEUS SSG dark matter detector, since minimum ionizing particles cause many granules to flip, while WIMPs cause only one granule to flip (flip meaning a transition from superconducting to normal state) [81]. In the following some of the most sensitive cryogenic WIMP detectors in operation are described.

The CDMS experiment [109] is located at the Soudan Underground Laboratory, USA, with an overburden of 2090 meter water equivalent (m.w.e.). In an early phase of the experiment the cryogenic detectors consisted of 4 towers of 250 g Ge absorbers which where read out by NTD germanium thermistors, so called Berkeley Large Ionization and Phonon (BLIP) detectors, and two towers of 100 g Si absorbers, which where read out by TES sensors, the so-called Z-sensitive Ionization and Phonon based (ZIP) detectors. The ZIP detectors utilize tungsten aluminum Quasi-particle trapping assisted Electrothermal feedback Transition edge sensors (QET). This type of sensor covers a large area of the Si absorber with aluminum phonon collector pads, where phonons are absorbed by breaking Cooper pairs and forming quasi-particles. The quasi-particles are trapped into a meander of tungsten strips which are used as transition edge sensors. The release of the quasi-particle energy in the tungsten strips increases their resistance, which will be observed as a current change in L detected with a SQUID as indicated in Fig. 19.3b. The transition edge device is voltage biased to take advantage of the electrothermal feedback (ETF). The signal pulses of the ZIP detector have rise times of a few µs and fall times of about 50 µs. They are much faster than the signals of the BLIP detector since the ZIP detectors are sensitive to the more energetic non thermal phonons. Their sensitivity to non thermal phonons and the pad structure of the sensors at the surface of the crystal allows for a localization of the event in the x-y plane. A separate circuit collects ionization charges, which are drifted by an electric field of 3 V/cm and collected on two concentric electrodes mounted on opposite sides of the absorber. The ratio of the ionization pulse height to the phonon pulse height versus the pulse height of the phonon detector allows to discriminate nuclear from electron recoils with a rejection factor better than 10^4 and with full nuclear recoil detection efficiency above 10 keV. In order to further improve the sensitivity of the experiment CDMS II is operating at present 19 Ge (250 g each) and 11 Si (100 g each) ZIP type detectors in the Soudan Underground Laboratory at a temperature of about 40 mK. Each detector is 7.62 cm in diameter and 1 cm thick. Limits on the direct detection of WIMPs obtained with the Ge and Si detectors are published in [110] and [111] respectively. The CDMSlite (Cryogenic Dark Matter Search low ionization threshold experiment) uses the Neganov-Luke effect, which leads to an amplification of the phonon signal and allows for lower energy thresholds (56 eV) to be reached [112–114]. In this mode a large detector bias voltage is applied to amplify the phonon signals produced by drifting quasi particle charges. This opens the possibility to extend the WIMP search to masses well below 10 GeV c^{-2}.

Recent results on low mass WIMP searches for spin independent and spin dependent interactions are published in [115].

The EDELWEISS experiment [116], which is located in the Frejus tunnel (4800 m.w.e.), South of France, uses a technique similar to the CDMS BLIP detectors. It consists of 3 towers of 320 g Ge absorbers which are read out by NTD germanium thermistors. For the ionization measurement the detectors are equipped with Al electrodes which are directly sputtered on the Ge absorber crystal. For some data taking runs the EDELWEISS group used towers with amorphous Ge and Si films under the Al electrodes. More data were collected between 2005 and 2011 with the EDELWEISS II detector which contains an array of ten cryogenic Ge detectors with a mass of 400 g each [117]. As an upgrade of EDELWEISS II the collaboration developed EDELWEISS III with 36 FID (Fully Inter-Digital) detectors based on cylindrical Ge crystals with a mass of about 800 g each operating at 18 mK [118].

Early experience with the ionization measurements showed a severe limitation of the background separation capability due to insufficient charge collection of surface events. The effect can be attributed to a plasma screening of the external electric field of the electrodes. As a result surface interactions of electrons can fake nuclear recoil events. One way to solve the problem was developed by the Berkeley group by sputtering films of amorphous Si or Ge on the absorber surface before deposition of the Al electrodes [119]. Due to the modified energy band gap of the amorphous layer the charge collection efficiency was largely improved. Fast phonon detectors like ZIP allow to identify surface events by measuring the relative timing between the phonon and ionization signals as demonstrated by the CDMS experiment [120]. The surface event problem completely disappears when using dual phonon-photon detection. This method was chosen by the CRESST II collaboration.

The CRESST experiment [121] is located in the Gran Sasso Underground Laboratory (3800 m.w.e.) north of Rome, Italy. It uses scintillating $CaWO_4$ crystals as absorber material. The detector structure can hold 33 modules of absorber which can be individually mounted and dismounted. Each module weights about 300 g. The detector operates at about 10 mK. The phonon signal from the $CaWO_4$ crystal is read by a superconducting tungsten TES thermometer and the photon signal by a separate but nearby cryogenic light detector, which consists of a silicon wafer with a tungsten TES thermometer. For an effective background discrimination the light detector has to be very efficient. This was achieved by applying an electric field to the silicon crystal leading to an amplification of the thermal signal due to the Neganov-Luke effect [122]. The time constant of the emission of scintillation photons from $CaWO_4$ at mK temperatures is of the order of ms, which requires a long thermal relaxation time for the light detector. The characteristics of the background rejection power depends on the knowledge of the quenching factor, which is the reduction factor of the light output of the nuclear recoil event relative to an electron event. These quenching factors were measured by the CRESST collaboration for various recoiling nuclei in $CaWO_4$ in a separate experiment [123]. The knowledge of these quenching factors would allow in principle to identify WIMP interactions with different nuclei in the $CaWO_4$ crystal. This method seems very promising, not only for identifying the background but also the quantum

numbers of the WIMP candidates. The three types of nuclei in $CaWO_4$ together with a low nuclear recoil energy threshold of 300 eV allowed CRESST II to extend the dark matter search with high sensitivity into a mass region below 10 GeV c^{-2} [124].

Besides the dark matter search the CRESST collaboration is developing a cryogenic detector to measure coherent neutrino nucleus scattering [125]. This process is predicted by the Standard Model (SM), but has been unobserved so far. If successful, a possible application could be the real time monitoring of nearby nuclear power plants. With a small size prototype cryogenic Saphire detector with a weight of 0.5 g a recoil energy threshold of 20 eV was achieved [126]. Nevertheless, the first detection of coherent neutrino scattering was reported from the COHERENT collaboration only recently [127]. They measured neutrino-induced recoils with conventional scintillating CsI(Na) crystals with a weight of 14.5 kg. Their experiment was located in a basement under the Oak Ridge National Laboratory Spallation Neutron Source.

The experimental results are usually presented as exclusion plots, which show the WIMP-nucleon cross section versus the WIMP mass. They are derived from the expected nuclear recoil spectrum for a given set of parameters [104]:

$$\frac{dR}{dE} = \frac{\sigma_0 \rho_\chi}{2\mu^2 m_\chi} F^2(E) \int_{\upsilon_{min}}^{\upsilon_{max}} \frac{f(\upsilon)}{\upsilon} d\upsilon \tag{19.17}$$

with m_χ the mass of the WIMP, μ the reduced mass of the WIMP-nucleus system, σ_0 the total elastic cross section at zero momentum transfer, $\rho_\chi = 0.3\,\mathrm{GeV\,cm^{-3}}$ the dark matter halo density in the solar neighborhood, $F(E)$ the nuclear form factor, $f(\upsilon)$ an assumed isothermal Maxwell-Boltzmann velocity distribution of the WIMPs in the halo, $\upsilon_{min} = \sqrt{E m_N / 2\mu^2}$ the minimum velocity which contributes to the recoil energy E, and $\upsilon_{max} = 575\,\mathrm{km\,s^{-1}}$ the escape velocity from the halo. The recoil energy E is given by $E = \mu^2 \upsilon^2 (1 - \cos\theta)/m_N$, with m_N the mass of the nucleus, υ the velocity of the WIMP, and θ the scattering angle in the centre of mass system. The expected nuclear recoil spectrum for interactions with WIMPs of a given mass will then be folded with the detector response, which was obtained experimentally from calibration measurements with neutron sources or in neutron beams. From a maximum likelihood analysis, an upper limit cross section value (90% C.L.) can be extracted for several different WIMP masses. Current limits for spin-independent WIMP interactions are depicted in Fig. 19.8, taken from [128]. The Figure includes only a selection of some of the most sensitive experiments. WIMP masses below 4 GeV c^{-2} are accessible by detectors like CRESST II [124], CDMSlite [115], EDELWEISS [118] and DAMIC [129] because of their low recoil energy thresholds and/or their light absorber nuclei. For WIMP masses above 6 GeV c^{-2} the best constraints are provided by experiments like XENON1T [130], LUX [131], PANDAX II [132], XENON 100 [133] and Dark Side 50 [134], which are based on massive dual phase (liquid and gas) Xenon or Argon detectors with time projection (TPC) read out. The DAMA experiment has observed

an annual modulation signal, which they claim is satisfying the requirements of a dark matter annual modulation signal [135]. Their detector is operated in the Gran Sasso Laboratory in Italy (LNGS) and is based on highly radiopure NaI (Tl) crystal scintillators. Similar results, but less significant, were reported by the CoGeNT experiment with a cryogenic Ge detector in the Soudan Underground Laboratory (SUL) [136]. Annual modulations have not been observed by other even more sensitive experiments and the interpretation of a WIMP signal is controversial. In order to better understand the origin of the observed modulation the SABRE experiment is planning to build twin detectors one of which will be placed in the northern hemisphere at the LNGS and the other in the southern hemisphere at the Stanwell Underground Physics Laboratory (SUPL) in Australia [137]. Both detectors will be identical and based on the same target material used in the DAMA experiment.

An extraction of the spin-dependent WIMP-nucleon cross section in a model independent way is not possible, since the nuclear and the SUSY degrees of freedom do not decouple from each other. Nevertheless, when using an "odd group" model which assumes that all the nuclear spin is carried by either the protons or the neutrons, whichever are unpaired, WIMP-nucleon cross sections can be deduced. The CDMSlite experiment [115] achieved constraints for spin dependent interactions below WIMP masses of 4 GeV c^{-2} complementary to LUX, PANDAX, XENON 100 and PICASSO [138].

Several experiments are planning to extend their sensitivity to a wide range of parameter space by operating multi tonnes of target material, reducing the energy thresholds and background level until the irreducible solar, earth and atmospheric neutrino background level is reached, Fig. 19.8. The EURECA (European Underground Rare Event Calorimeter) will bring together researchers from the CRESST

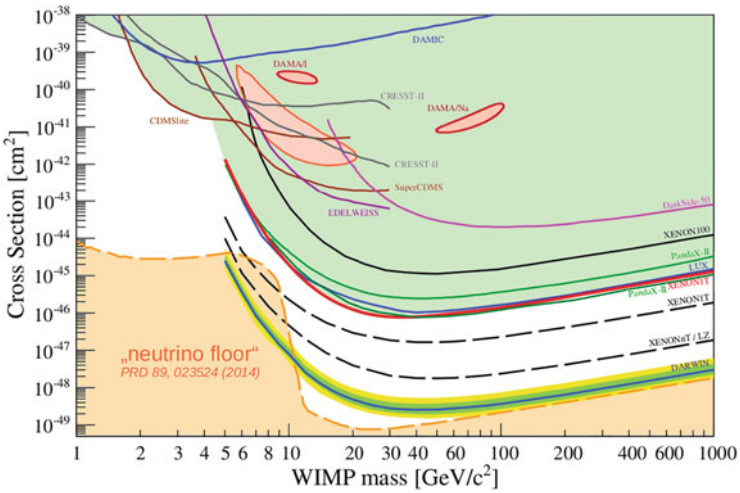

Fig. 19.8 Current limits for spin-independent WIMP interactions are shown

and EDELWEISS experiments to built a 1 ton cryogenic detector in the Modane Underground Laboratory in France [139]. SUPER CDMS will be operated in the Sudbury Neutrino Observatory (SNOLab) in Canada and is based on cryogenic Ge and Si absorber materials to increase their sensitivity for dark matter interaction cross sections to 10^{-43} cm^2 for masses down to 1 GeV c^{-2} [140]. The Dark Side 50 collaboration is planning to built a 23 ton dual phase liquid Argon TPC to be operated at the LNGS. The LUX-ZEPLIN (LZ) experiment is currently under construction in the Sanford Laboratory in South Dakota. It uses 10 ton of liquid XENON (dual phase) in a radio-poor double vessel cryostat [142]. The ultimate WIMP detector is proposed by the DARWIN collaboration at the LNGS [141]. It will be based on multi tonnes of liquid Xenon and will fill almost the entire parameter space for spin independent WIMP interaction cross sections down to the background level of neutrino interactions in the detector material as shown in Fig. 19.8. The ambitious project will also be sensitive to other rare interactions like solar axions, galactic axion like particles, neutrinoless double beta decay in ^{136}Xe and coherent neutrino nucleus scatterings.

19.5.2 Neutrino Mass Studies

Since the discovery of neutrino oscillations by the Kamiokande and Super-Kamiokande experiments [143] a new chapter in physics started. These findings showed that neutrinos have a mass and that there is new physics to be expected beyond the Standard Model (SM) in particle physics. Among the most pressing questions remain the absolute values of the neutrino masses, since from oscillation experiments only mass differences can be obtained [144], and the Dirac or Majorana type character of the neutrino. The main streams in this field focus upon the search for the neutrinoless double beta decay and the endpoint energy spectrum of beta active nuclei. Cryogenic detectors are particularly well suited for this type of research since they provide excellent energy resolutions, an effective background discrimination and a large choice of candidate nuclei.

19.5.2.1 Neutrinoless Double Beta Decay

Double beta decay was first suggested in 1935 by Maria Goeppert Mayer [145]. It is the spontaneous transition from a nucleus (A,Z) to its isobar (A,Z+2). This transition can proceed in two ways: (A,Z)⇒(A,Z+2) + 2 e^- + 2 $\bar{\nu}_e$ or (A,Z)⇒(A,Z+2) + 2 e^-. In the first channel, where two electrons and two antineutrinos are emitted, the lepton number is conserved. It is the second channel, the neutrinoless double beta decay ($0\nu\beta\beta$), where the lepton number is violated. In this case, with no neutrino in the final state, the energy spectrum of the decay would show in a peak which represents the energy sum of the two electrons. The experimental observation of this process would imply that neutrinos are Majorana particles, meaning that the

neutrino is not distinguishable from its antiparticle and that it has a non-vanishing mass. From the measured decay rate $(1/T^{0\nu}_{1/2})$ one can derive in principle its effective mass $< m_\nu >$ or a lower limit of it:

$$(1/T^{0\nu}_{1/2}) = G_{0\nu}(E_0, Z) \mid M_{0\nu} \mid^2 < m_\nu >^2 \tag{19.18}$$

where $G_{0\nu}(E_0, Z)$ is an accurately calculable phase space function and $M_{0\nu}$ is the nuclear matrix element, which is not very well known [146]. The calculated values of $M_{0\nu}$ can vary by factors up to two. Consequently the search for $0\nu\beta\beta$ should be made with several different nuclei in order to confirm an eventual discovery of this important process.

The Milano group has developed an experiment with the name CUORICINO to search for the neutrinoless double beta decay of ^{130}Te. The experiment is located in the Gran Sasso Underground Laboratory. The detector consists of an array of 62 TeO_2 crystals with the dimensions $5 \times 5 \times 5\,cm^3$ (44 crystals) and $3 \times 3 \times 3\,cm^3$ (18 crystals) and a total mass of 40.7 kg. The crystals are cooled to ~8 mK and attached to Ge NTD thermistors for phonon detection. Among other possible nuclear candidates (like for example $^{48}CaF_2$, ^{76}Ge, $^{100}MoPbO_4$, $^{116}CdWO_4$, $^{150}NdF_3$, $^{150}NdGaO_3$), $^{130}TeO_2$ was chosen because of its high transition energy of 2528.8 ± 1.3 keV and its large isotopic abundance of 33.8%. Published first results of the CUORICINO experiment [147] show no evidence for the $0\nu\beta\beta$ decay, but they set a lower limit on the half lifetime $T^{0\nu}_{1/2} \geq 1.8 \cdot 10^{24}$ yr (90% C.L.) corresponding to $< m_\nu > \leq$ 0.2 to 1.1 eV (depending on nuclear matrix elements). In a next step the collaboration developed CUORE-0 as prototype for a larger detector CUORE. Its basic components consist of 52 TeO_2 crystals with dimensions $5 \times 5 \times 5\,cm^3$ and a total weight of 39 kg corresponding to 10.9 kg ^{130}Te. CUORE-0 was operated in the CUORICINO cryostat at 12 mK. The data taken from 2013 to 2015 show no evidence for a neutrinoless double beta signal. Combined with the CUORICINO results a limit on the half lifetime $T^{0\nu}_{1/2} \geq 4 \cdot 10^{24}$ yr (90% C.L.) corresponding to $< m_\nu > \leq$ 270 to 760 meV (depending on nuclear matrix elements) was achieved [148]. CUORE, contains 19 CUORE-0 type towers with 988 TeO_2 crystals of a total mass of 741 kg corresponding to 206 kg of ^{130}Te [149, 150]. The array will be cooled in a large cryostat to 10 mK. It started commissioning early 2017 and aims for a sensitivity to reach limits of $T^{0\nu}_{1/2} \geq 9 \cdot 10^{25}$ yr in 5 years running time [150]. For the future the CUPID collaboration plans to develope a tonne-scale cryogenic detector which will be based on the experience gained with the CUORE experiment [151].

Several experiments investigated other nuclei and set stringent upper limits on the decay rates, for example: KamLand-Zen in ^{136}Xe [152], EXO-200 in ^{136}Xe [153], GERDA in ^{76}Ge [154], NEMO-3 in ^{100}Mo [155]. So far no neutrinoless double beta signal was seen. Currently a limit on the half lifetime $T^{0\nu}_{1/2} \geq 1.07 \cdot 10^{26}$ yr (90% C.L.) corresponding to $< m_\nu > \leq$ 60 to 165 meV (depending on nuclear matrix elements) was achieved by the KamLand-Zen experiment. An ambitious alternative approach in looking for Majorana versus Dirac type neutrinos is proposed by the

PTOLEMY experiment in studying the interaction of cosmic relic neutrinos with Tritium [156].

19.5.2.2 Direct Neutrino Mass Measurements

So far the best upper limit for the electron neutrino mass of 2.2 eV was obtained from the electron spectroscopy of the tritium decay $^3\mathrm{H} \Rightarrow {}^3\mathrm{He} + e^- + \bar{\nu}_e$, with a transition energy of 18.6 keV, by the Mainz and the Troitsk experiments [157]. In the near future the KATRIN experiment, which measures the same decay spectrum with a much improved electron spectrometer, will be in operation aiming for a neutrino mass sensitivity down to 0.2 eV [158].

One of the problems with experiments based on a spectroscopic measurement of the emitted electrons is that they yield negative values for the square of the neutrino mass when fitting the electron energy spectrum. This is mainly due to final state interactions (like tritium decays into excited atomic levels of ^{3}He), which lead to deviations from the expected energy spectrum of the electron. Low temperature calorimeters provide an alternative approach, since they measure the total energy including final state interactions, such as the de-excitation energy of excited atomic levels. However, in order to reach high sensitivity for low neutrino masses the detector has to have an excellent energy resolution and enough counting rate statistics at the beta endpoint energy. The Genoa group [159] pioneered this approach and studied the beta decay of $^{187}\mathrm{Re} \Rightarrow {}^{187}\mathrm{Os} + e^- + \bar{\nu}_e$ with a cryogenic micro-calorimeter. Their detector was a rhenium single crystal (2 mg) coupled to a Ge NTD thermistor. Rhenium is a super-conductor with a critical temperature of 1.7 K. Natural Re contains 62.8% of ^{187}Re with an endpoint energy of about 2.6 keV. The operating temperature of the detector was $T = 90$ mK. In their first attempt they obtained precise values for the beta endpoint energy and the half life of the ^{187}Re beta decay and were able to obtain an upper limit of the electron neutrino mass of 19 eV (90% CL) or 25 eV (95% CL) [160]. Following this approach the Milan group [161] has built an array of ten thermal detectors for a ^{187}Re neutrino mass experiment. The detectors were made from $AgReO_4$ crystals with masses between 250 and 350 µg. The crystals were coupled to Si implanted thermistors. Their average energy resolution (FWHM) at the beta endpoint was 28.3 eV, which was constantly monitored by means of fluorescence X-rays. The natural fraction of ^{187}Re in $AgReO_4$ yields a decay rate of $5.4 \cdot 10^{-4}$ Hz/µg. From a fit to the Curie plot of the ^{187}Re decay they obtained an upper limit for $m_{\bar{\nu}_e} \leq 15$ eV. Their measured value for the beta endpoint energy is 24653.3 ± 2.1 eV and for the half live is $(43.2 \pm 0.3) \cdot 10^9$ yr. A higher sensitivity to low neutrino masses may be achievable in the future, provided that the energy resolution and the statistics at the beta endpoint energy can be improved significantly. The latter may raise a problem for thermal phonon detectors, since their signals are rather slow and therefore limit the counting rate capability to several Hz.

With their Rhenium cryogenic micro-calorimeters the Genoa group [162, 163] and the Milano collaboration [164] were also able to measure interactions between

the emitted beta particle and its local environment, known as beta environmental fine structure (BEFS). The BESF signal originates from the interference of the outgoing beta electron wave and the reflected wave from the atoms in the neighbourhood. BEFS is similar to the well known Extended X-ray Absorption Fine Structure (EXAFS) method. Their results demonstrated that cryogenic micro-calorimeters may also offer complementary new ways for material sciences to study molecular and crystalline structures.

Currently several groups MARE [165, 166], ECHo [167], HOLMES [168], NUMECS [169], are investigating the possibility to measure the electron neutrino mass from the Electron Capture (EC) decay spectrum of Holmium (^{163}Ho) using cryogenic micro-calorimeters. This approach was originally suggested by A. de Rujula and M. Lusignoli in 1982 [170]. ^{163}Ho decays via EC into ^{163}Dy with a half life of 4570 years and a decay energy of 2.833 keV. It does not occur naturally and it is not commercially available. It has to be produced by neutron or proton irradiation. After purification the ^{163}Ho atoms have to be implanted into a suitable absorber material of the micro-calorimeter. In order to reach a neutrino mass sensitivity in the sub-eV region a total ^{163}Ho activity of several MBq is required. Since the activity of a single micro-calorimeter should not exceed 100 Bq the total ^{163}Ho activity has to be distributed over a large number of pixels (10^5). The groups are devoting much effort in developing micro-calorimeters with energy and time resolutions of the order of 1 eV and 1 µs respectively. Various thermal sensors, like TES, MMC and MKID, are considered. Multiplexing schemes have still to be invented to be able to read out the enormous number of pixels.

As already mentioned above, an upper limit for all neutrino masses of $\sum m_\nu \leq 0.234\,\mathrm{eV\,c^{-2}}$ was derived from cosmology. It will still take some efforts to reach or go below these limits in the near future with direct mass measurements. A review of direct neutrino mass searches can be found in [171].

19.5.3 Astrophysics

Modern astrophysics addresses a large list of topics: Formation of galaxies and galaxy clusters, the composition of the intergalactic medium, formation and evolution of black holes and their role in galaxy formation, matter under extreme conditions (matter in gravitational fields near black holes, matter inside neutron stars), supernovae remnants, accretion powered systems with white dwarfs, interstellar plasmas and cosmic microwave background radiation (CMB). The investigation of these topics requires optical instruments with broad band capability, high spectral resolving power, efficient photon counting and large area imaging properties. The radiation received from astrophysical objects spans from microwaves, in the case of CMB, to high energy gamma rays. The subjects discussed here can be divided into three categories, X-ray, optical/ultraviolet (O/UV) and CMB observations. In order to avoid the absorptive power of the earth atmosphere many of the instruments are operated in orbiting observatories, in sounding rockets or in balloons. Progress in

this rapidly growing field of science is constantly asking for new instrumentation and new technologies. Cryogenic detectors are playing a key role in these developments providing very broad-band, imaging spectrometers with high resolving power. They also feature high quantum efficiencies, single photon detection and timing capabilities. The observation of large-scale objects, however, needs spatial-spectral imaging devices with a wide field of view requiring cryogenic detectors to be produced in large pixel arrays. The fabrication and the readout of these arrays remains still a big challenge.

19.5.3.1 X-Ray Astrophysics

The orbital X-ray observatories Chandra and XMM-Newton contained CCD cameras for large field imaging and dispersive spectrometers for narrow field high spectral resolution. Cryogenic devices are able to combine both features in one instrument. Although they have not yet reached the imaging potential of the 2.5 megapixel CCD camera on XMM-Newton and the resolving power $E/\Delta E_{FWHM} = 1000$ at $E = 1\,\mathrm{keV}$ of the dispersive spectrometer on Chandra, their capabilities are in many ways complementary. For example, the resolving power of cryogenic devices increases with increasing energy and is above 2 keV better than the resolving power of dispersive and grating spectrometers, which decreases with increasing energy. Since the cryogenic pixel array provides a complete spectral image of the source at the focal plane its resolving power is independent of the source size. Cryogenic detectors also provide precise timing information for each photon allowing to observe rapidly varying sources such as pulsars, etc. They cover a wide range of photon energies (0.05–10 keV) with a quantum efficiency of nearly 100%, which is 5 times better than the quantum efficiency (20%) of CCDs.

The first space-borne cryogenic X-ray Quantum Calorimeter (XQC), a collaboration between the Universities of Wiskonsin, Maryland and the NASA Goddard Space Flight Center, was flown three times on a sounding rocket starting in 1995 [172]. The rockets achieved an altitude of 240 km providing 240 s observation above 165 km per flight. The XQC was equipped with a 2×18 micro-calorimeter array consisting of HgTe X-ray absorbers and doped silicon thermistors yielding an energy resolution of 9 eV across the spectral band. The pixel size was $1\,\mathrm{mm}^2$. The micro-calorimeters were operated at 60 mK. It is interesting to note that, when recovering the payload after each flight, the dewar still contained some liquid helium. The purpose of the mission was to study the soft X-ray emission in the band of 0.03–1 keV. The physics of the diffuse interstellar X-ray emission is not very well understood. It seems that a large component is due to collisional excitations of particles in an interstellar gas with temperatures of a few 10^6 K. A detailed spectral analysis would allow to determine the physical state and the composition of the gas. Since the interstellar gas occupies a large fraction of the volume within the galactic disk, it plays a major role in the formation of stars and the evolution of the galaxy. The results of this experiment and their implications are discussed in [172]. As a next step the Japan-USA collaboration has put an X-ray spectrometer

(XRS) on board of the Astro-E2 X-ray Suzaku satellite which was launched in July 2005. This instrument is equipped with 32 pixels of micro-calorimeters (HgTe) and semiconducting thermistors and is an improvement over the XQC spectrometer in terms of fabrication techniques, thermal noise, energy resolution of 7 eV across the operating band of 0.03–10 keV and observation time [173, 174]. The pixels are 0.624 mm^2 and arranged in a 6×6 array giving a field of view of 2.9×2.9 arcmin. The observatory is looking at the interstellar medium in our and neighboring galaxies as well as at supernovae remnants. The investigations include super massive black holes and the clocking of their spin rate.

The next step is to develop cryogenic detectors with increased pixel numbers (30×30) and energy resolutions of 2 eV, which would be able to replace dispersive spectrometers in future experiments. Superconducting micro-calorimeters with TES sensors have the potential to reach energy resolutions of 2 eV and are likely to replace semiconducting thermistors. One of the problems with cryogenic detectors is that they do not scale as well as CCDs, which are able to clock the charges from the center of the arrays to the edge using a serial read out. Cryogenic detectors rely on individual readout of each pixel. Another problem is the power dissipation in large arrays. To solve some of these problems, dissipation-free metallic magnetic calorimeters (MMC) and microwave kinetic inductance detectors (MKID) [80] are among the considered possibilities. Details of these new developments can be found in the proceedings of LTD. Large cryogenic detector arrays are planned for ATHENA (Advanced Telescope for High Energy Astrophysics), a future X-ray telescope of the European Space Agency. It is designed to investigate the formation and evolution of large scale galaxy clusters and the formation and grows of super massive black holes. The launch of ATHENA is planned for 2028.

19.5.3.2 Optical/UV and CMB Astrophysics

Since the first optical photon detection with STJ's in 1993 [175] and TES's in 1998 [176] a new detection concept was introduced in the field of Optical/UV astrophysics. Further developments demonstrated the potential of these single photon detection devices to combine spectral resolution, time resolution and imaging in a broad frequency band (near infrared to ultraviolet) with high quantum efficiency. The principle of these spectrophotometers is based on the fact that for a superconductor with a gap energy of typically 1 meV an optical photon of 1 eV represents a large amount of energy. Thus a photon impinging on a superconductor like for example Ta creates a large amount of quasi-particles leading to measurable tunnel current across a voltage biased junction. A first cryogenic camera S-Cam1 with a 6×6 array of Ta STJs (with a pixel size of $25 \times 25\,\mu m^2$) was developed by ESTEC/ESA and 1999 installed in the 4 m William Herschel telescope on La Palma (Spain) [75]. For a first proof of principle of this new technique the telescope was directed towards the Crab pulsar with an already known periodicity of 33 ms. The photon timing information was recorded with a 5 µs accuracy with respect to the GPS timing signals. Following the success of the demonstrator model S-Cam1

and of the improved model S-Cam2 a new camera S-Cam3 consisting of a 10×12 Ta STJ pixel array (with pixel dimension $33 \times 33\,\mu m^2$) was installed at the ESA 1m Optical Ground Station Telescope in Tenerife (Spain). The STJ structure is 100 nm Ta/30 nm Al//AlOx//30 nm Al/100 nm Ta. The camera covers a wavelength range of 340–740 nm with a wavelength resolution of 35 nm at $\lambda = 500$ nm and has a pulse decay time of 21 µs [177]. The Stanford-NIST (National Institute of Standards and Technology) collaboration has also developed a camera with an 8×8 pixel array based on tungsten TES sensors on a Si substrate [178]. Each pixel has a sensitive area of $24 \times 24\,\mu m^2$ and the array has a $36 \times 36\,\mu m$ center to center spacing. In order to improve the array fill factor a reflection mask is positioned over the inter-pixel gaps. For both STJ and TES spectro-photometers thermal infrared (IR) background radiation, which increases rapidly with wavelength above 2 µm, is of concern. Special IR blocking filters have to be employed in order to extend the wavelengths range of photons from 0.3 µm out to 1.7 µm. A 4 pixel prototype of the Stanford-NIST TES instrument was already mounted at the 2.7 m Smith Telescope at McDonald Observatory (U.S.A) and observed a number of sources including spin powered pulsars and accreting white dwarf systems. The Crab pulsar served as a source to calibrate and tune the system. The obtained data are published in [179]. Already these first results have shown that STJ or TES based spectrophotometers are in principal very promising instruments to study fast time variable sources like pulsars and black hole binaries as well as faint objects, like galaxies in their state of formation. However, in order to extend the observations from point sources to extended objects much larger pixel arrays are required. Future developments concentrate on a suitable multiplexing system in order to increase the number of pixels, which are presently limited by the wiring on the chip and the size of the readout electronics. SQUID multiplexing readout systems [180–182] as well as Distributed Read-out Imaging Devices (DROID) [74, 183], in which a single absorber strip is connected to two separate STJs on either side to provide imaging capabilties from the ratio of the two signal pulses, are under study. However, these devices are slower than small pixel devices and can handle only lower count rates. A much faster device is the superconducting MKID detector [80], which allows a simple frequency-domain approach to multiplexing and profits from the rapid advances in wireless communication electronics. A more detailed review can be found in [184, 185]. A camera, ACRONS, for optical and near infrared spectroscopy has been developed. The camera contains a 2024 pixel array of cryogenic MIKD detectors. The device is able to detect individual photons with a time resolution of 2 µs and simultaneous energy information [80]. The instrument has been used for optical observations of the Crab pulsar [186].

Large cryogenic pixel antennas have been developed for ground-based and space-borne CMB polarization measurements. These devices aim to be sensitive to the detection of the so-called primordial E- and B-modes, which would appear as curling patterns in the polarization measurements. E-modes arise from the density perturbations while B- modes are created by gravitational waves in the early universe. The two modes are distinguishable through their characteristic patterns. However, B-mode signals are expected to be an order of magnitude weaker than E-

modes. Nevertheless, B-modes are of particular interest since they would provide revealing insight into the inflationary scenario of the early universe signaling the effect of primordial gravity waves. There are several instruments, which use TES based cryogenic bolometers, in operation: EBEX [187] and SPIDER [188] are balloon-borne experiments, overflying the Antarktis. POLARBEAR [189] is an instrument, which is coupled to the HUAN TRAN Teleskope at the James Ax Observatory in Chile. BICEP2 and the Keck Array [190] are located at the Amundsen-Scott South Pole Station. The PLANCK Satellite [191] carried 48 cryogenic bolometers operating at 100 mK in outer space. In March 2014 the BICEP2 collaboration reported the detection of B-modes [190]. However the measurement was received with some skepticism and David Spergel argued that the observation could be the result of light scatterings off dust in our galaxy. In September 2014 the PLANCK team [191] concluded that their very accurate measurement of the dust is consistent with the signal reported by BICEP2. In 2015 a joint analysis of BICEP2 and PLANCK was published concluding that the signal could be entirely attributed to the dust in our galaxy [192].

19.6 Applications

Electron probe X-ray microanalysis (EPMA) is one of the most powerful methods applied in material sciences. It is based on the excitation of characteristic X-rays of target materials by high current electron beams in the energy range of several keV. EPMA finds its application in the analysis of contaminant particles and defects in semiconductor device production as well as in the failure analysis of mechanical parts. It is often used in the X-ray analysis of chemical shifts which are caused by changes in the electron binding due to chemical bonding as well as in many other sciences (material, geology, biology and ecology). The X-rays are conventionally measured by semiconducting detectors (Si-EDS), which are used as energy dispersive spectrometers covering a wide range of the X-ray spectrum, and/or by wavelength dispersive spectrometers (WDS). Both devices have complementary features. WDS, based on Bragg diffraction spectrometry, has a typical energy resolution of 2–15 eV (FWHM) over a large X-ray range. However, the diffraction limits the bandwidth of the X-rays through the spectrometer as well as the target size, which acts as a point source, and makes serial measurements necessary, which is rather time consuming. Contrary, the Si-EDS measures the entire X-ray spectrum from every location of the target simultaneously, but with a typical energy resolution of 130 eV. Si-EDS is therefore optimally suited for a quick but more qualitative analysis. Cryogenic micro-calorimeter EDS provides the ideal combination of the high resolution WDS and the broadband features of the energy dispersive EDS. The application of cryogenic detectors for EPMA was first introduced by Lesyna et al. [193]. The NIST group developed a prototype TES based micro-calorimeter which is suitable for industrial applications [42, 194, 195]. It consists of a Bi absorber and a Al-Ag or Cu-Mo bi-layer TES sensor. It covers

an area of $0.4 \times 0.4\,\mathrm{mm}^2$ and yields an energy resolution of 2 eV at 1.5 keV and 4.5 eV at 6 keV. The detector is cooled to 100 mK by a compact adiabatic demagnetization refrigerator and is mounted on a scanning electron microscope. Cryogenic refrigerators for this and various other applications are commercially available [196]. In spite of its excellent resolving power (see Fig. 19.2) the micro-calorimeter EDS has still two shortcomings. It has a limited counting rate capability (1 kHz compared to 100 kHz WDS and 25 kHz Si-EDS) and a small effective detector surface. To compensate for the latter the NIST group developed an X-ray focusing device using poly-capillary optics. The device consists of many fused tapered glass capillaries which focus the X-rays by means of internal reflection onto the micro-calorimeter increasing its effective area. Another solution under study is a multiplexed micro-calorimeter array with a possible loss in resolution due to the variability of individual detectors [182]. Nevertheless, TES based cryogenic micro-calorimeters EDS have already demonstrated major advances of EPMA in scientific and industrial applications.

Time of flight mass spectrometry (ToF-MS) of biological molecules using cryogenic detectors was first introduced by D. Twerenbold [197]. The main advantage of cryogenic calorimeters over traditionally employed micro-channel plates (MP) is that the former are recording the total kinetic energy of an accelerated molecule with high efficiency, independent of its mass, while the efficiency of the latter is decreasing with increasing mass due to the reduction of the ionization signal. ToF-MS equipped with MP lose rapidly in sensitivity for masses above 20 kDa (proton masses). The disadvantages of cryogenic detectors are: first, they cover only a rather small area of $\sim 1\,\mathrm{mm}^2$ while a MP with $4\,\mathrm{cm}^2$ will cover most of the beam spot size of a spectrometer; second, the timing signals of the cryogenic calorimeters are in the range of µs and therefore much slower than ns signals from MP, which degrades the flight time measurements and thus the accuracy of the molecular mass measurements. A good review of early developments can be found in [198]. After the early prototype experiences made with STJs [199, 200] and NIS (Normal-conductor/Isolator/Super-conductor) tunnel junctions [201], which provided only very small impact areas, super-conducting phase transition thermometers (SPT) with better time of flight resolutions and larger impact areas of $3 \times 3\,\mathrm{mm}^2$ were developed [202–204]. These devices consist of thin super-conducting Nb meanders, or super-conducting films in thermal contact with an absorber, which are current biased and locally driven to normal conducting upon impact of an ion. A voltage amplifier is used to measure the signal pulse.

Cryogenic detectors as high resolution γ-ray, α and neutron spectrometers also found applications in nuclear material analysis, as broad band micro-calorimeters in Electron Beam Ion Traps (EBITs) and in synchrotrons for fluorescence-detected X-ray absorption spectroscopy (XAS) [202]. They are also employed in nuclear and heavy ion physics [205].

19.7 Summary

Cryogenic detectors have been developed to explore new frontiers in astro and particle physics. Their main advantages over more conventional devices are their superior energy resolution and their sensitivity to very low energy transfers. However, most thermal detectors operate at mK temperatures requiring complex refrigeration systems and they have limited counting rate capabilities (1 Hz–1 kHz). Today the most frequently used thermometers for calorimeters operating in near equilibrium mode are doped semiconductors (thermistors), superconducting transition edge sensors (TES) and metallic paramagnets (MMC). Because they are easy to handle and commercially available thermistors are quite popular. They have, however, the disadvantage of having to deal with Joule heating introduced by their readout circuit. The most advanced technology is provided by the TES sensors in connection with an auto-biasing electrothermal feedback system. This system reduces the effect of Joule heating, stabilizes the operating temperature and is self-calibrating, which turns out to be advantageous also for the operation of large detector arrays. The main advantage of MMCs is their magnetic inductive readout, which does not dissipate power into the system. This feature makes MMC attractive for applications, where large detector arrays are required. Non-equilibrium detectors like superconducting tunnel junctions (STJ), superheated superconducting granules (SSG) and microwave kinetic inductance devices (MKID) are based on the production and detection of quasi-particles as a result of Cooper pair breaking in the superconductor. These devices are intrinsically faster, providing higher rate capabilities (10 kHz and more) and good timing properties suitable for coincident measurements with external detectors. Because of their sensitivity to low energy photons arrays of STJs are frequently employed in infrared and optical telescopes, but also efficiently used in x-ray spectroscopy. SSG detectors with inductive readout have the potential to reach very low energy thresholds (order of several eV) which would be advantageous for various applications like for example in neutrino physics (coherent neutrino scattering, etc.). But the practical realization of SSG detectors is still very challenging. MKIDs provide an elegant way to readout large detector arrays by coupling an array of many resonators with slightly different resonance frequencies to a common transmission line with a single signal amplifier. Due to this feature they are very suited for the future instrumentation of astrophysical observatories and other applications. Cryogenic calorimeters with a large detector mass for dark matter searches and neutrino physics as well as large detector arrays for astrophysical measurements and other practical applications are under intense developments. Despite the enormous progress made in the past their fabrication and readout remain still a challenge.

References

1. S.P. Langley, Proc. Am. Acad. Arts Sci. **16** (1881) 342.
2. P. Curie, A. Laborde, Compt.Rend. Hebd. Seances Acad. Sci. Paris **136** (1903) 673–675.
3. C.D. Ellis, A. Wooster, Proc. R. Soc. **117** (1927) 109–123.
4. W. Orthmann, Z. Phys. **60** (1930) 10; and L. Meitner, W. Orthmann, Z. Phy. **60** (1930) 143.
5. F. Simon, Nature **135** (1935) 763.
6. D.H. Andrews, R.D. Fowler, M.C. Williams, Phys.Rev. **76** (1949) 154.
7. G.H. Wood, B.L. White, Appl. Phys. Lett. **15** (1969) 237; and G.H. Wood, B.L. White, Can. J. Phys. **51** (1973) 2032.
8. H. Bernas et al., Phys. Lett. A **24** (1967) 721.
9. A. Drukier, C. Vallette, Nucl. Instrum. Meth. **105** (1972) 285.
10. A. Drukier, L. Stodolsky, Phys. Rev. D **30** (1984) 2295.
11. N. Coron, G. Dambier, J. Leblanc, in: *Infrared detector techniques for Space Research*, V. Manno, J. Ring (eds.), Reidel Dordrecht (1972), pp. 121–131.
12. T.O. Niinikoski, F. Udo, CERN NP Report 74–6 (1974).
13. E. Fiorini, T.O. Niinikoski, Nucl. Instrum. Meth. **224** (1984) 83.
14. D. McCammon, S.H. Moseley, J.C. Mather, R. Mushotzky, J. Appl. Physics **56**(5) (1984) 1263.
15. N. Coron et al., Nature **314** (1985) 75–76.
16. K. Pretzl, N. Schmitz, L. Stodolsky (eds.), Low-Temperature Detectors for Neutrinos and Dark Matter LTD1, Schloss Ringberg, Germany, Springer-Verlag (1987).
17. L. Gonzalez-Mestres, D. Perret-Gallix (eds.), Low-Temperature Detectors for Neutrinos and Dark Matter LTD2, Gif-sur-Yvette, France, Ed. Frontieres (1988).
18. L. Brogiato, D.V. Camin, E. Fiorini (eds.), Low-Temperature Detectors for Neutrinos and Dark Matter LTD3, Gif-sur-Yvette, France, Ed. Frontieres (1989).
19. N.E. Booth, G.L. Salmon (eds.), Low Temperature Detectors for Neutrinos and Dark Matter LTD4, Gif-sur-Yvette, France, Ed. Frontieres (1992).
20. S.E. Labov, B.A. Young (eds.), Proc. 5th Int. Workshop Low Temperature Detectors LTD5, Berkeley, CA, J. Low Temp. Phys. **93**(3/4) (1993) 185–858.
21. H.R. Ott, A. Zehnder (eds.), Proc. 6th Int. Workshop Low Temperature Detectors LTD6, Beatenberg/Interlaken, Switzerland, Nucl. Instrum. Meth. A **370** (1996) 1–284.
22. S. Cooper (ed.), Proc. 7th Int. Workshop Low Temperature Detectors LTD7, Max Planck Institut of Physics Munich, Germany, ISBN 3-00-002266-X, (1997).
23. P. deKorte, T. Peacock (eds.), Proc. 8th Int. Workshop Low Temperature Detectors LTD8, Dalfsen, Netherlands, Nucl. Instrum. Meth. A **444** (2000).
24. F. Scott Porter, D. MacCammon, M. Galeazzi, C. Stahle (eds.). Proc. 9th Int. Workshop Low Temperature Detectors LTD9, American Institute of Physics AIP Conf. Proc. **605** (2002).
25. F. Gatti (ed.), Proc. 10th Int. Workshop Low Temperature Detectors LTD10, Genova, Italy, Nucl. Instrum. Meth. A **520** (2004).
26. M. Ohkubo (ed.), Proc. 11th Int. Workshop Low Temperature Detectors LTD11, Tokyo, Japan, Nucl. Instrum. Meth. A **559** (2006).
27. M. Chapellier, G. Chardin (eds.), Proc. 12th Int. Workshop Low Temperature Detectors LTD12, Paris, France, J. Low Temp. Phys. **151**(1/2, 3/4) (2008).
28. B. Cabrerra, A. Miller, B.Young (eds.), Proc. 13th Int.Workshop Low Temperature Detectors LTD13, Stanford/SLAC, USA, American Inst. of Physics (March 2010).
29. Ch. Enss, A. Fleischmann, L. Gastaldo (eds.), Proc. 14th Int.Workshop Low Temperature Detectors LTD14, Heidelberg, Germany, J.Low Temp.Phys.**167**(5/6) (2012) 561–1196.
30. E. Skirokoff(ed.), Proc. 15th Int.Workshop Low Temperature Detectors LTD15, Pasadena Cal., USA, J. Low Temp. Phys.**176**(3/6)(2014) 131–1108.
31. Ph. Camus, A. Juillard, A. Monfardini (eds.), Proc. 16th Int.Workshop Low Temperature Detectors LTD16, Grenoble, France, J. Low Temp. Phys. **184**(1/4)(2016) 1–978.

32. A. Barone (ed.), Proc. Superconductive Particle Detectors, Torino, Oct. 26–29, 1987, World Scientific.
33. A. Barone, Nucl. Phys. B (Proc. Suppl.) **44** (1995) 645.
34. D. Twerenbold, Rep. Prog. Phy. **59** (1996) 349.
35. H. Kraus, Supercond. Sci. Technol. **9** (1996) 827.
36. N. Booth, B. Cabrera, E. Fiorini, Annu. Rev. Nucl. Part. Sci. **46** (1996) 471.
37. K. Pretzl, *Cryogenic calorimeters in astro and particle physics*, Nucl. Instrum. Meth. A **454** (2000) 114.
38. Ch. Enss (ed.), *Cryogenic particle detection*, Topics in Applied Physics Vol. **99**, Springer Berlin, Heidelberg, New York (2005).
39. D. McCammon, *Thermal Equilibrium Calorimeters-An Introduction*, in: *Cryogenic particle detection*, Topics in Applied Physics Vol. **99**, Ch. Enss (ed.), Springer Berlin, Heidelberg, New York (2005), p. 1.
40. J.C. Mather, Appl. Opt. **21** (1982) 1125.
41. S.H. Moseley, J.C. Mather, D. McCammon, J. Appl. Phys. **56**(5) (1984) 1257–1262.
42. D.A. Wollmann et al., Nucl. Instrum. Meth. A **444** (2000) 145.
43. T.C.P. Chui et al., Phys. Rev. Lett. **69**(21) (1992) 3005.
44. B.I. Shklovskii, A.L. Efros, *Electronic Properties of Doped Semiconductors*, Springer-Verlag (1984).
45. P. Colling et al., Nucl. Instrum. Meth. A **354** (1995) 408.
46. K.D. Irwin, Appl. Phys. Lett. **66** (1995) 1998.
47. K.D. Irwin, G.C. Hilton, *Transition Edge Sensors*, in: *Cryogenic particle detection*, Topics in Applied Physics Vol. **99**, Ch. Enss (ed.), Springer Berlin, Heidelberg, New York (2005), p. 63.
48. B. Young et al., IEEE Trans. Magnetics **25** (1989) 1347.
49. K.D. Irwin, B. Cabrera, B. Tigner, S. Sethuraman, in: Proc. 4th Int. Workshop Low Temperature Detectors for Neutrinos and Dark Matter LTD4, N.E. Booth, G.L. Salmon (eds.), Gif-sur-Yvette, France, Ed. Frontieres (1992), p. 290.
50. P. Ferger et al., Nucl. Instrum. Meth. A **370** (1996) 157.
51. P. Colling et al., Nucl. Instrum. Meth. A **354** (1995) 408.
52. U. Nagel et al., J. Appl. Phys. **76** (1994) 4262.
53. J. Hohne et al., X-Ray Spectrom. **28** (1999) 396.
54. J. Martinis, G. Hilton, K. Irwin, D. Wollmann, Nucl. Instrum. Meth. A **444** (2000) 23.
55. G. Brammertz et al., Appl. Phys. Lett. **80** (2002) 2955.
56. C. Hunt et al., Proc. SPIE **4855** (2003) 318.
57. B. Young et al., Nucl. Instrum. Meth. A **520** (2004) 307.
58. M. Buehler, E. Umlauf, Europhys. Lett. **5** (1988) 297.
59. E. Umlauf, M.Buehler, in: Proc. Int. Workshop Low Temperature Detectors for Neutrinos and Dark Matter LTD4, N.E. Booth, G.L. Salmon (eds.), Gif-sur-Yvette, France, Ed. Frontieres (1992), p. 229.
60. S.R. Bandler et al., J. Low Temp. Phys. **93** (1993) 709.
61. A. Fleischmann et al., Nucl. Instrum. Meth. A **520** (2004) 27.
62. A. Fleischmann, C. Enss, G.M. Seidel, *Metallic Magnetic Calorimeters*, in: *Cryogenic particle detection*, Topics in Applied Physics Vol. **99**, Ch. Enss (ed.), Springer Berlin, Heidelberg, New York (2005), p. 196.
63. A. Barone, G. Paterno, Physics and Applications of the Josephson Effect, New York, Wiley-Interscience (1984).
64. D. Twerenbold, A. Zehnder, J. Appl. Phys. **61** (1987) 1.
65. H. Kraus et al., Phys. Lett. B **231** (1989) 195.
66. C.A. Mears, S. Labov, A.T. Barfknecht, Appl. Phys. Lett. **63** (21) (1993) 2961.
67. P. Lerch, A. Zehnder, *Quantum Giaever Detectors: STJ's*, in: *Cryogenic particle detection*, Topics in Applied Physics Vol. **99**, Ch. Enss (ed.), Springer Berlin, Heidelberg, New York (2005), p. 217.
68. N.E. Booth, Appl. Phys. Lett. **50** (1987) 293.

69. K.E. Gray, Appl. Phys. Lett. **32** (1978) 392.
70. I. Giaever, K. Megerle, Phys. Rev. **122**(4) (1961) 1101.
71. S.B. Kaplan et al., Phys. Rev. B **14**(11) (1976) 4854.
72. P.A.J. de Korte et al., Proc. SPIE **1743** (1992) 24.
73. G. Angloher et al., J. Appl. Phys. **89**(2) (2001) 1425.
74. P. Verhoeve et al., Proc. SPIE **6276** (2007) 41.
75. N. Rando et al., Rev. Sci. Instrum. **71**(12) (2000) 4582.
76. R. Christiano et al., Appl. Phys. Lett. **74** (1999) 3389.
77. M.P. Lissitski et al., Nucl. Instrum. Meth. A **520** (2004) 240.
78. E. Figueroa-Feliciano, Nucl. Instrum. Meth. A **520** (2004) 496.
79. P.K. Day et al., Nature **425** (2003) 871.
80. B. Mazin et al., Publ.Astro.Soc. of the pacific **125** (2013) 1348–1361.
81. K. Borer et al., Astroparticle Phys. **22** (2004) 199.
82. K. Borer, M. Furlan, Nucl. Instrum. Meth. A **365** (1995) 491.
83. A. Kotlicki et al., in: Low-Temperature Detectors for Neutrinos and Dark Matter LTD1, K. Pretzl, N. Schmitz, L. Stodolsky (eds.) Springer-Verlag (1987), p. 37.
84. R. Leoni et al., J. Low Temp. Phys. **93**(3/4) (1993) 503.
85. B. van den Brandt et al., Nucl. Phys. B (Proc. Suppl.) **70** (1999) 101.
86. M. Abplanalp et al., Nucl. Instrum. Meth. A **360** (1995) 616.
87. S. Janos et al., Nucl. Instrum. Meth. A **547** (2005) 359.
88. G. Meagher et al., J. Low Temp. Phys. **93**(3/4) (1993) 461.
89. C. Berger et al., J. Low Temp. Phys. **93**(3/4) (1993) 509.
90. S. Calatroni et al., Nucl. Instrum. Meth. A **444** (2000) 285.
91. S. Casalboni et al., Nucl. Instrum. Meth. A **459** (2001) 469.
92. S. Calatroni et al., Nucl. Instrum. Meth. A **559** (2006) 510.
93. M. Abplanalp, Nucl. Instrum. Meth. A **370** (1996) 11.
94. K. Pretzl, Particle World **1**(6) (1990) 153.
95. K. Pretzl, J. Low Temp. Phys. **93** (1993) 439.
96. F. Zwicky, Helv. Phys. Acta **6** (1933) 110.
97. S. Perlmutter et al., Astrophys. J. **483** (1997) 565.
98. A.G. Riess et al., Astronom. J. **116** (1998) 1009.
99. The Planck collaboration (P.Ade et al.), Astronom. Astrophys. **594**A (13) (2016) and arXiv: 1502.01589 (astro-phys.Co) (2016)
100. R.D. Peccei, H.R. Quinn, Phys. Rev. Lett. **38** (1977) 1440.
101. P.W. Graham et al., An.Rev.Nucl. and Particle Searches **65** (2015) 485–514 and arXiv: 1602.00039 (hep - ex) (2016)
102. F.Kahlhofer, Int.J.Mod.Phys. A **32** (2017) 1730006 and arXiv: 1702.02430 (hep - ph)
103. K. Pretzl, Space Science Reviews **100** (2002) 209.
104. G. Jungman, M. Kamionkowski, K. Griest, Phys. Rep. **267** (1996) 195.
105. B. Sadoulet, in: Low Temperature Detectors for Neutrinos and Dark Matter LTD1, K. Pretzl, L. Stodolsky, N. Schmitz (eds.), Springer-Verlag (1987), p. 86.
106. L. Gonzalez-Mestres, D. Perret-Gallix, Nucl. Instrum. Meth. A **279** (1989) 382.
107. S. Cebrian et al., Phys. Lett. B **563** (2003) 48.
108. P. Meunier et al., Appl. Phys. Lett. **75**(9) (1999) 1335.
109. D.S. Akerib et al., Phys. Rev. D **72** (2005) 052009.
110. Z.Ahmed et al., Phys. Rev. Lett. **106** (2011) 131302 and R.Agnese et al., Phys. Rev. D **92** (7) (2015) 072003 and arXiv:1504.05871 (hep-ex).
111. R.Agnese et al., Phys. Rev. Lett. **111** (2013) 251301 and arXiv:1304.4279 (hep-ex).
112. N.Luke, J. Appl. Phys. **64** (1988) 6858.
113. G. Wang, J. Appl. Phys. **107** (2010) 094504.
114. C. Isaila et al.,Phys. Lett. B **716** (2012) 160.
115. R. Agnese et al.,Phys. Rev. Lett. **116** (7) (2016) 071301, R.Agnese et al., arXiv:1707.01632 (2017) submitted to Phys. Rev. D.
116. V. Sanglard et al., Phys. Rev. D **71** (2005) 122002.

117. E.Armengaud et al.,Phys.Lett. B **702** (2011) 329–335 and arXiv:1103.4070 (astro-ph.Co) (2011)
118. L.Hehn et al., Eur. Phys. J. C **76** (10) (2016) 548 and arXiv: 1607.03367 (astro-ph.Co) (2016), E.Armengaud et al., arXiv 1706.01070 (physics.ins-det) (2017)
119. T. Shutt et al., Nucl. Instrum. Meth. A **444** (2000) 34.
120. D.S. Akerib et al., Phys. Rev. D **68** (2003) 082002.
121. G. Angloher et al., Astroparticle Physics **31** (2009) 270–276 and arXiv:0809.1829 [astro-ph].
122. C. Isaila et al., Nucl. Instrum. Meth. **559** (2006) 399; and C. Isaila et al., J. Low Temp. Phys. **151**(1/2) (2008) 394.
123. J. Ninković et al., Nucl. Instrum. Meth. A **564** (2006) 567.
124. G. Angloher et al., Eur.Phys. J.C **76** (1) (2016) 25 and arXiv: 1509.01515.
125. R. Strauss et al., Eur.Phys. J.C bf77 (2017) 506 and arXiv: 1704.04320 (physics.ins-det) (2017).
126. R. Strauss et al., Phys.Rev. D bf96 (2) (2017) 022009 and arXiv: 1704.04317.
127. D. Akimov et al., Science **357** (2017) 1123
128. Mark Schumann, Physics Departement University Freiburg Germany, private communication.
129. A. Aguilar-Arevalo et al., Phys. Rev. D **94** (2016) 082006 and arXiv: 1607.07410.
130. E. Aprile et al., arXiv: 1705.06655.
131. D. Akerib et al., Phys. Rev. Lett. **118** (2) (2017) 021303 and arXiv: 1608.07648.
132. A. Tan et al., Phys. Rev. Lett. **117** (12) (2016) 12133 and arXiv: 1708.06917.
133. E. Aprile et al., Phys. Rev. D **94** (12) (2016) 122001 and arXiv: 1609.06154.
134. P. Agnes et al., Phys. Lett. B **743** (2015) 456–466 and arXiv:1410.0653.
135. R.Bernabei et al., Eur. Phys.J.Web Conf **13** (2017) 60500 and arXiv:1612.01387 R.Bernabei et al. Eur. Phys. J. C **73** (2013) 2648.
136. C. E. Aalseth et al., Phys. Rev. Lett. **106** (13) (2011) 131301 and arXiv:1401.3295.
137. F.Froborg et al.,arXiv:1601.05307.
138. E. Behnke et al., Astropart. Phys. **90** (2017) 85–92.
139. G. Agloher et al.,Phys.Dark Univ. **3** (2014) 41–74.
140. R.Agnese et al.,Phys. Rev. D **95** (8) (2017) 082002 and arXiv: 1610.0006.
141. J.Aalbers et al., JCAP **11** (2016) 017 and arXiv: 1606.07001.
142. D.S.Akerib et al., Astropart. Phys. **96** (2017) 1–10
143. Y. Fukuda et al., Phys. Rev. Lett. **81**(8) (1998) 1562.
144. M. Maltroni, T. Schwetz, M. Tortola, J.W.F. Valle, New J. Phys. **6** (2004) 122.
145. M. Goeppert Mayer, Phys. Rev. **48** (1935) 512.
146. P. Vogel, *Double Beta decay: Theory, Experiment and Implications*, in: *Current aspects of Neutrino Physics*, D.O. Caldwell (ed.), Springer-Verlag (2001), p. 177.
147. C. Arnaboldi et al., Phys. Rev. Lett. **95** (2005) 142501.
148. K.Alfonso et al., Phys. Rev. Lett. **115** (10) (2015) 102502 and arXiv: 1504.02454 (nucl.-ex).
149. C.Alduino et al., J.INST **11** (7) (2016) P07009 and arXiv: 1604.05465 (phys.ins-det) (2016).
150. C.Alduino et al., Eur. Phys. J. C **77** (8) (2017) 532 and arXiv: 1705.10816 (phys.ins-det) (2017).
151. G.Wang et al., arXiv: 1504.03599 (phys. ins.-det) (2015)
152. A.Gaudo et al., Phys. Rev. Lett. **110** (2013) 062502 and arXiv: 1605.02889 (2016)
153. J.B. Albert et al., Nature **510** (2014) 229
154. M. Agostini et al., Nature **544** (2017) 5
155. R.Arnold et al., Phys. Rev. D **92** (2015) 072011
156. S.Betts et al., arXiv: 1307.4738 (astro-ph.IM) (2013)
157. V.M. Lobashov, Nucl. Phys. A **719** (2003) 153, and references therein.
158. KATRIN experiment, https//www.katrin.kit.edu.
159. F. Fontanelli, F. Gatti, A. Swift, S. Vitale, Nucl. Instrum. Meth. A **370** (1996) 247.
160. F. Gatti et al., Nucl. Phys. B **91** (2001) 293.

161. M. Sisti et al., Nucl. Instrum. Meth. A **520** (2004) 125.
162. F. Gatti et al., Nature **397** (1999) 137.
163. F. Gatti, F. Fontanelli, M. Galeazzi, S. Vitale, Nucl. Instrum. Meth. A **444** (2000) 88.
164. C. Arnaboldi et al., Phys. Rev. Lett. **96** (2006) 042503.
165. A. Nucciotti, J. Low Temp. Phys. **151**(3/4) (2008) 597.
166. E. Ferri et al.,J. Low Temp. Phys. **176** (5/6) (2014) 885–890.
167. L. Gastaldo et al.,J. Low Temp. Phys. **176** (5/6) (2014) 876–884.
168. B.Alperit et al., The European Physical Journal C **75** (2015) 112.
169. M.P. Croce et al., J.Low Temp. Phys. **184** (3/4) (2016) 958–968 and arXiv:1510.03874.
170. A. de Rujula and M. Lusignoli, Phys. Lett. B **118** (1982) 429434.
171. O. Dragoun and D. Vnos, Open Physics Journal **3** (2016) 73–113.
172. D. McCammon et al., Astrophys. J **576** (2002) 188.
173. C.K. Stahle et al., Nucl. Instrum. Meth. A **520** (2004) 466.
174. D.D.E. Martin et al., Nucl. Instrum. Meth. A **520** (2004) 512.
175. N. Rando et al., J. Low Temp. Phys. **93**(3/4) (1993) 659.
176. B. Cabrera et al., Appl. Phys. Lett. **73** (1998) 735.
177. D.D.E. Martin et al., Proc. SPIE **6269** (2006) 62690O-1.
178. J. Burney et al., Nucl. Instrum. Meth. A **559** (2006) 506.
179. R.W. Romani et al., Astrophys. J. **563** (2001) 221.
180. J.A. Chervanek et al., Appl. Phys. Lett. **44** (1999) 4043.
181. P.A.J. de Korte et al., Rev. Sci. Instrum. **74**(8) (2003) 3807.
182. W.B. Doriese et al., Nucl. Instrum. Meth. A **559** (2006) 808.
183. R.A. Hijemering et al., Nucl. Instrum. Meth. A **559** (2006) 689.
184. B. Cabrera, R. Romani, *Optical/UV Astrophysics Applications of Cryogenic detectors*, in: *Cryogenic particle detection*, Topics in Applied Physics Vol. **99**, Ch. Enss (ed.), Springer Berlin, Heidelberg, New York (2005), p. 416.
185. P. Verhoeve, J. Low Temp. Phys. **151**(3/4) (2008) 675.
186. M.J.Strader et al. Astrophys. J. Letters **779** (2013) L12.
187. Asad M. Aboobaker et al., arXiv: 1703.03847 (astro-phys.IM) (2017).
188. J.M.Nagy et al., Astrophysics J. **844** (2) (2017) 151 and arXiv:1704.0025.
189. P.Ade et al., The Astrophysical Journal **794** (171) (2014) 21.
190. P.A.R. Ade et al., Phys. Rev. Lett. **112** (24) (2014) 241101.
191. PLANCK Collaboration, Astronomy & Astrophysics **586** (2014) A133.
192. P.A.R. Ade et al. Phys. Rev. Lett. **114** (10) (2015) 101301 and arXiv:1502.00612.
193. L. Lesyna et al., J. Low Temp. Phys. **93** (1993) 779.
194. R. Ladbury, Physics Today (July 1998) 19.
195. D.E. Newbury et al., *Electron Probe Microanalysis with Cryogenic Detectors*, in: *Cryogenic particle detection*, Topics in Applied Physics Vol. **99**, Ch. Enss (ed.), Springer Berlin, Heidelberg, New York (2005), p. 267.
196. V. Shvarts et al., Nucl. Instrum. Meth. A **520** (2004) 631.
197. D. Twerenbold, Nucl. Instrum. Meth. A **370** (1996) 253.
198. M. Frank et al., Mass Spectrometry Reviews **18** (1999) 155.
199. D. Twerenbold et al., Proteomics **1** (2001) 66.
200. M. Frank et al., Rapid Commun. Mass Spectrom. **10**(15) (1996) 1946.
201. G.C. Hilton et al., Nature **391** (1998) 672.
202. J.N. Ullom, J. Low Temp. Phys. **151**(3/4) (2008) 746.
203. S. Rutzinger et al., Nucl. Instrum. Meth. A **520** (2004) 625.
204. P. Christ et al., Eur. Mass Spectrom. **10** (2004) 469.
205. P. Egelhof, S. Kraft-Bermuth, *Heavy Ion Physics*, in: *Cryogenic particle detection*, Topics in Applied Physics Vol. **99**, Ch. Enss (ed.), Springer Berlin, Heidelberg, New York (2005), p. 469.